LETTER

EZH2 inhibition as a therapeutic strategy for lymphoma with EZH2–activating mutations

Michael T. McCabe[1], Heidi M. Ott[1], Gopinath Ganji[1], Susan Korenchuk[1], Christine Thompson[1], Glenn S. Van Aller[1], Yan Liu[1], Alan P. Graves[2], Anthony Della Pietra III[1], Elsie Diaz[2], Louis V. LaFrance[1], Mark Mellinger[1], Celine Duquenne[1], Xinrong Tian[1], Ryan G. Kruger[1], Charles F. McHugh[1], Martin Brandt[2], William H. Miller[1], Dashyant Dhanak[1], Sharad K. Verma[1], Peter J. Tummino[1] & Caretha L. Creasy[1]

In eukaryotes, post-translational modification of histones is critical for regulation of chromatin structure and gene expression. EZH2 is the catalytic subunit of the polycomb repressive complex 2 (PRC2) and is involved in repressing gene expression through methylation of histone H3 on lysine 27 (H3K27). EZH2 overexpression is implicated in tumorigenesis and correlates with poor prognosis in several tumour types[1–5]. Additionally, somatic heterozygous mutations of Y641 and A677 residues within the catalytic SET domain of EZH2 occur in diffuse large B-cell lymphoma (DLBCL) and follicular lymphoma[6–10]. The Y641 residue is the most frequently mutated residue, with up to 22% of germinal centre B-cell DLBCL and follicular lymphoma harbouring mutations at this site. These lymphomas have increased H3K27 tri-methylation (H3K27me3) owing to altered substrate preferences of the mutant enzymes[9,11–13]. However, it is unknown whether specific, direct inhibition of EZH2 methyltransferase activity will be effective in treating EZH2 mutant lymphomas. Here we demonstrate that GSK126, a potent, highly selective, S-adenosyl-methionine-competitive, small-molecule inhibitor of EZH2 methyltransferase activity, decreases global H3K27me3 levels and reactivates silenced PRC2 target genes. GSK126 effectively inhibits the proliferation of EZH2 mutant DLBCL cell lines and markedly inhibits the growth of EZH2 mutant DLBCL xenografts in mice. Together, these data demonstrate that pharmacological inhibition of EZH2 activity may provide a promising treatment for EZH2 mutant lymphoma.

To identify inhibitors of EZH2 methyltransferase activity, a high-throughput biochemical screen with a five-member PRC2 protein complex was performed[14]. This work identified a small-molecule EZH2 inhibitor with a $K_i^{app} = 700$ nM. Extensive optimization of this compound through medicinal chemistry generated GSK126 (Fig. 1a). GSK126 potently inhibits both wild-type and mutant EZH2 methyltransferase activity with similar potencies ($K_i^{app} = 0.5–3$ nM) independent of substrate used, and is competitive with S-adenosyl-methionine (SAM) and non-competitive with peptide substrates (Fig. 1b and Supplementary Fig. 1a, b). GSK126 is highly selective against other methyltransferases and multiple other protein classes (Supplementary Tables 1–4). In particular, GSK126 is more than 1,000-fold selective for EZH2 versus 20 other human methyltransferases, including both SET-domain-containing and non-SET-domain-containing methyltransferases[15]. Even EZH1, which is 96% identical to EZH2 within the SET domain, and 76% identical overall, is inhibited more than 150-fold less potently ($K_i^{app} = 89$ nM). Using an EZH2 homology model[9], combined with enzyme mechanism-of-action and inhibitor structure–activity relationship data, *in silico* docking revealed the SAM binding pocket as the most plausible docking site for GSK126. Here it is predicted to make extensive contacts with the post-SET domain which forms one side of the SAM binding pocket (Supplementary Fig. 2a–d). Interestingly, within 10 Å of the predicted GSK126-binding site, four of the six residue differences between EZH2 and EZH1 lie within the post-SET domain, and these may contribute to the decreased potency for EZH1.

The altered substrate preferences of EZH2 mutants lead to an imbalance in cellular H3K27 methylation states (Supplementary Fig. 3a)[9,11]. Nonetheless, GSK126 induced a 50% loss of H3K27me3 in both EZH2 wild-type and mutant DLBCL cell lines at concentrations ranging from 7–252 nM independent of EZH2 mutation status (t-test, $P = 0.27$) (Fig. 1c). Further analyses demonstrated that inhibition of H3K27me3 began before 24 h and potency was maximal after 2 days (Supplementary Fig. 3b). GSK126 most potently inhibited H3K27me3, followed by H3K27me2, and H3K27me1 was only weakly reduced at the highest inhibitor concentration (Fig. 1d and Supplementary Fig. 3c). Total histone H3 and PRC2 components were not affected by GSK126 (Supplementary Figs 3c and 4), thus reduction of H3K27 methylation is due to direct inhibition of EZH2 methyltransferase activity and not degradation of histone H3 or PRC2.
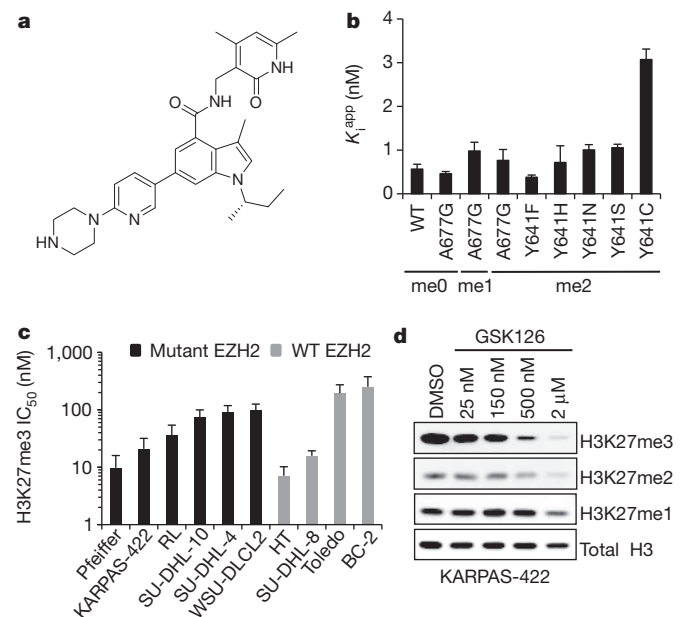
Figure 1 | Biochemical and cellular mechanistic activity of GSK126.
a, Structure of GSK126. **b**, Potency of GSK126 against wild-type and mutant EZH2. Histone H3 peptides (21–44) with K27me0, K27me1 or K27me2 were used as substrates ($n = 2$; mean values ± s.d. are shown). **c**, Effect of GSK126 on H3K27me3 in lymphoma cell lines treated with GSK126 for 48 h. IC50 values were determined using an H3K27me3 ELISA ($n \geq 2$; mean values ± s.d. are shown). **d**, Evaluation of H3K27me3/2/1 in KARPAS-422 cells following treatment for 72 h. Total histone H3 is shown as a loading control.

[1]Cancer Epigenetics Discovery Performance Unit, Cancer Research, Oncology R&D, GlaxoSmithKline, 1250 S. Collegeville Road, Collegeville, Pennsylvania 19426, USA. [2]Platform Technology and Sciences, GlaxoSmithKline, 1250 S. Collegeville Road, Collegeville, Pennsylvania 19426, USA.

This is in contrast to 3-deazaneplanocin A (DZNep), an inhibitor of S-adenosyl-L-homocysteine (SAH) hydrolase that promotes degradation of the PRC2 complex and indirectly inhibits EZH2 through effects on intracellular SAH concentrations[16].

We evaluated the effect of GSK126 on cell proliferation in a panel of B-cell lymphoma cell lines. DLBCL cell lines were the most sensitive to EZH2 inhibition (Fig. 2a). Six of the seven most sensitive DLBCL cell lines harboured Y641N, Y641F or A677G EZH2 mutations (growth $IC_{50} = 28$–861 nM) (Fig. 2a, Supplementary Table 5 and Supplementary Fig. 5). The exception was the cell line HT, which is wild type for EZH2 (growth $IC_{50} = 516$ nM). Interestingly, HT harbours a mutation in UTX (R1111C), a H3K27 demethylase frequently inactivated in multiple tumour types[17]. Only two of the 11 remaining DLBCL cell lines harboured EZH2 mutations indicating that, in most cases, DLBCL cell lines with mutant EZH2 are dependent on EZH2 activity for cell growth. However, in some situations co-occurring

alterations may override the dependence of the cell on EZH2 activity, making it less sensitive to EZH2 inhibition. Among EZH2 mutant cell lines, sensitivity to GSK126 is independent of BCL2 translocation or p53 mutation, common alterations found within DLBCL (Supplementary Table 5). There was a modest correlation between inhibition of H3K27me3 and cell growth (Pearson, $r = 0.62$), but there was no correlation between sensitivity to GSK126 and EZH2 protein levels (Supplementary Fig. 6a–c). Interestingly, two of the most sensitive DLBCL cell lines, WSU-DLCL2 and KARPAS-422, are derived from patients with refractory disease[18,19] indicating that DLBCL cells that are resistant to standard-of-care may be sensitive to EZH2 inhibition. Burkitt lymphoma and Hodgkin's lymphoma cell lines were generally less sensitive to EZH2 inhibition (growth $IC_{50} > 1.3\,\mu M$) with the exception of Jiyoye (growth $IC_{50} = 232$ nM), a Burkitt lymphoma cell line with wild-type EZH2. Evaluation of GSK126 in additional lymphoma cell lines and extensive genomic and epigenomic
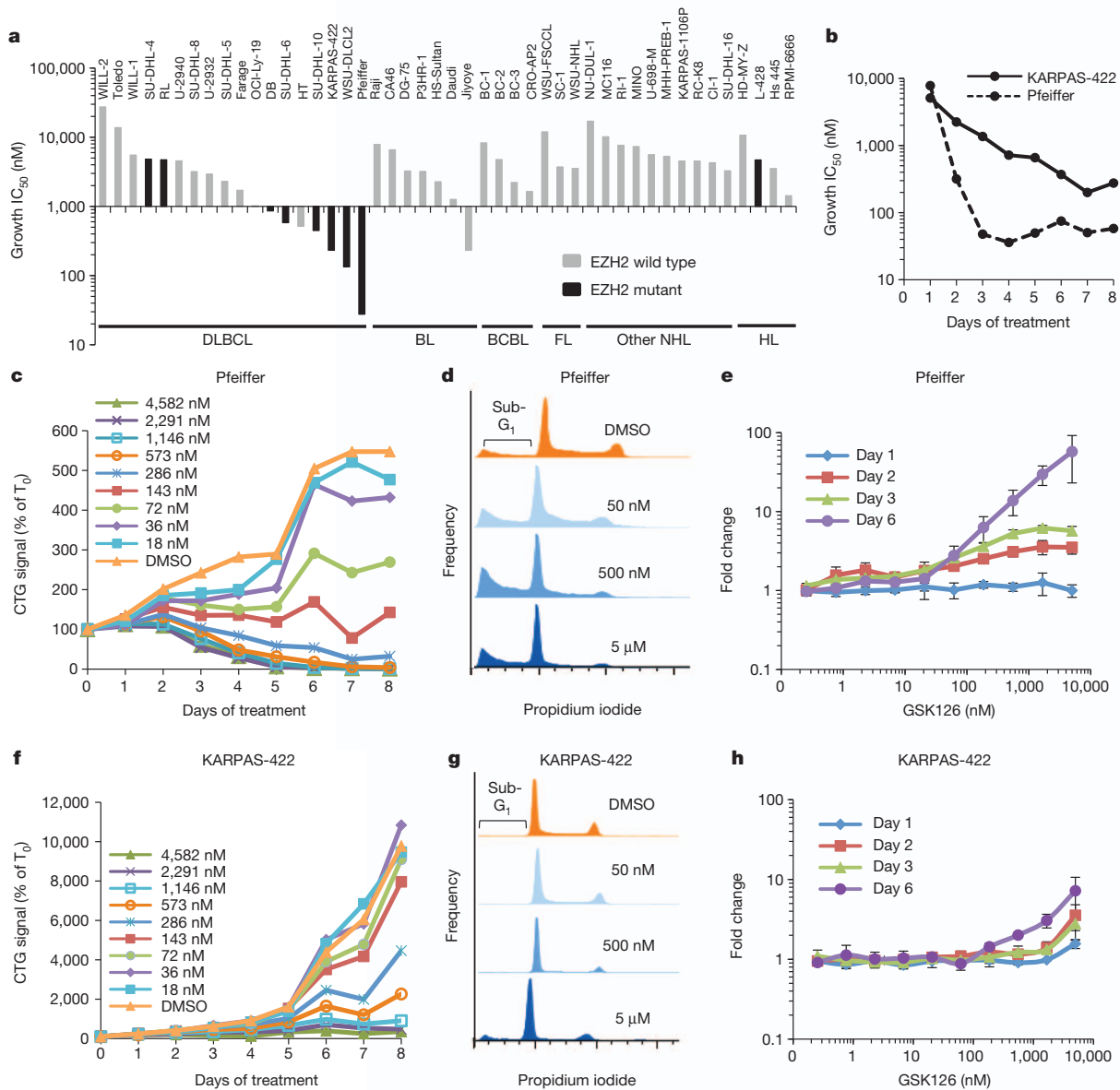
Figure 2 | GSK126 inhibits the proliferation of several EZH2 mutant lymphoma cell lines. a, The effect of GSK126 on the growth of 46 lymphoma cell lines after 6 days represented as the concentration of GSK126 required to inhibit 50% of growth (growth IC_{50}). BCBL, AIDS body cavity-based lymphoma; BL, Burkitt lymphoma; DLBCL, diffuse large B-cell lymphoma; FL, follicular lymphoma; HL, Hodgkin's lymphoma; NHL, non-Hodgkin's lymphoma. **b**, Potency of GSK126 on growth of Pfeiffer and KARPAS-422 cells over time represented as growth IC_{50}. **c, f**, Dose-dependent effects of GSK126 on cell proliferation over time in Pfeiffer or KARPAS-422 cells. Growth is expressed as a percentage of CTG at time zero (T_0). **d, g**, DNA content histograms showing the effect of GSK126 on the cell cycle after 72 h. **e, h**, Mean fold-change in caspase 3/7 activity over vehicle control $\pm$ s.d. is shown ($n = 4$).

characterization will be required to fully elucidate the determinants of sensitivity among lymphoma subtypes.

Both cytostatic and cytotoxic responses were observed among the most sensitive cell lines (Supplementary Table 5); therefore, the timing of GSK126-induced effects on proliferation and cell death was examined in detail in two of the most sensitive cell lines. In the Pfeiffer cell line, potent inhibition of cell proliferation was observed after 2 days (Fig. 2b) and net decreases in cell number were evident after 3 days (Fig. 2c). This cell death seems to be driven by caspase-mediated apoptosis as indicated by the increase in the sub-G_1 population (Fig. 2d) and dose-dependent induction of caspase activity (Fig. 2e). The response in the KARPAS-422 cell line was slower with 6–7 days required for maximal potency (Fig. 2b). Furthermore, a primarily cytostatic effect was observed in KARPAS-422 cells as demonstrated by CellTiter-Glo (CTG) values remaining above day 0 levels, a G_1 arrest (43% and 77% of cells in G_1 with dimethylsulphoxide (DMSO) and 500 nM GSK126, respectively) with little sub-G_1 content, and minimal caspase activity with $<1\,\mu M$ GSK126 (Fig. 2f–h). Consistent with these observations, short-hairpin-RNA-mediated knockdown of EZH2 led to profound cytotoxic and apoptotic responses in Pfeiffer cells, and decreased cell proliferation and no caspase

activation in KARPAS-422 cells, demonstrating that the phenotypic effects observed with GSK126 are due to inhibition of EZH2 (Supplementary Fig. 7).

Because EZH2 is associated with transcriptional repression, we evaluated the effect of GSK126 on gene expression in DLBCL cell lines with a range of sensitivity to GSK126. Robust transcriptional activation was noted in the most sensitive cell lines (Fig. 3a, Supplementary Fig. 8a and Supplementary Table 6). Not surprisingly, considering the repressive nature of H3K27me2/3, the majority of transcriptional changes involved upregulation. The high degree of similarity between gene expression changes observed with GSK126 treatment and EZH2 knockdown in KARPAS-422 and Pfeiffer cells indicates that these transcriptional changes are due to loss of EZH2 activity and not off-target effects (Supplementary Figs 9 and 10). Additionally, analysis of data from chromatin immunoprecipitation followed by sequencing (ChIP-seq) for the three most responsive cell lines showed that before treatment upregulated genes exhibited broad enrichment of H3K27me3, indicating that these genes are EZH2 targets marked by H3K27me3 (Fig. 3b and Supplementary Fig. 11).

In contrast to the response observed in the sensitive cell lines, minimal transcriptional changes occurred with GSK126 treatment in
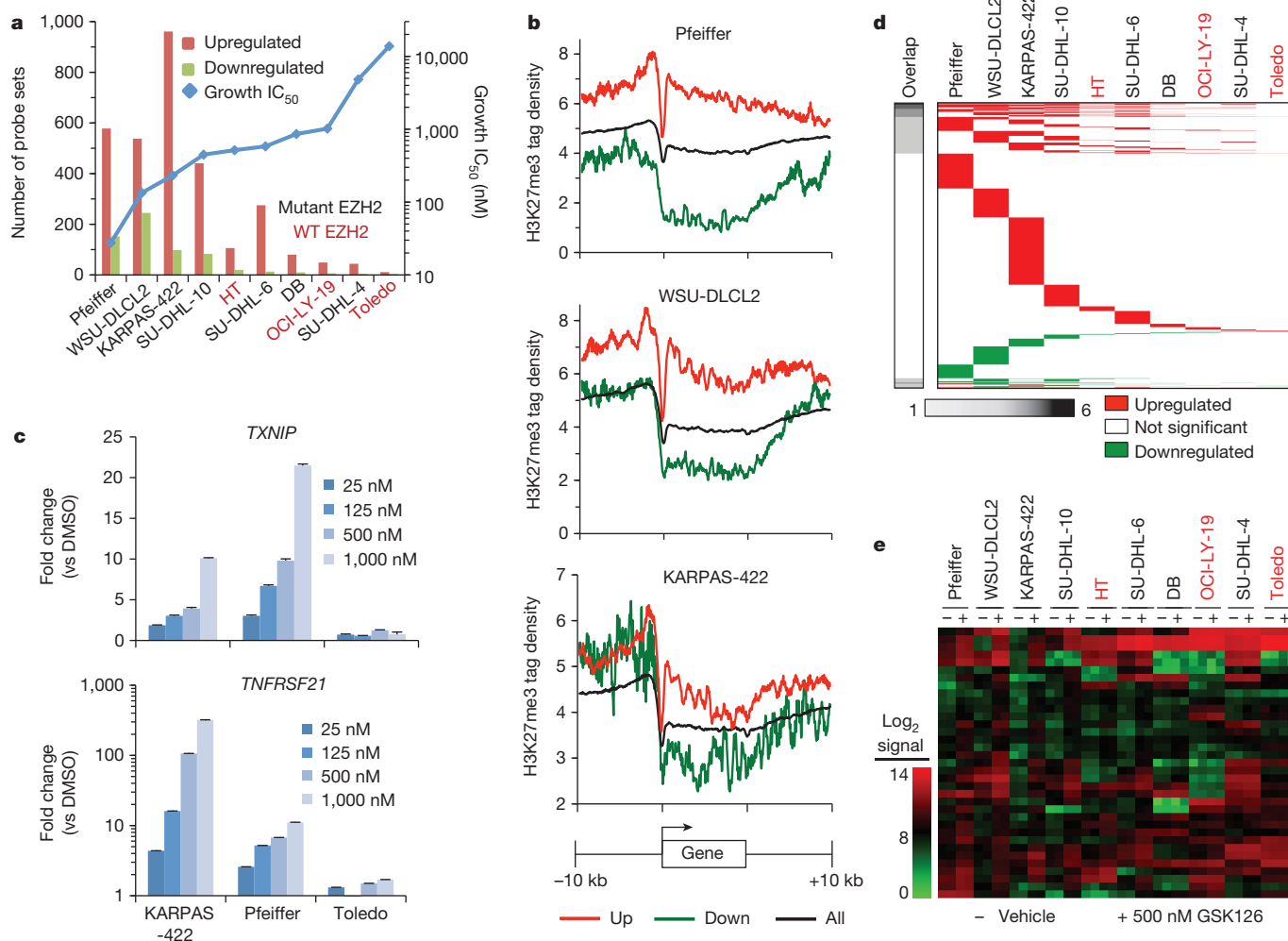
Figure 3 | GSK126 induces transcriptional activation in sensitive cell lines. a, The number of probe sets showing significantly altered gene expression (false discovery rate (FDR) < 0.1 and fold-change > 2 or < −2) following 72 h treatment with 500 nM GSK126 ($n = 2$). **b**, Basal H3K27me3 ChIP-seq enrichment profiles of genes upregulated (red), downregulated (green), or all human transcripts (black) following GSK126 treatment. **c**, qRT–PCR analysis of *TXNIP* and *TNFRSF21* following 72 h treatment with GSK126 ($n = 3$; mean

values ± s.d. are shown). **d**, The overlap of up- and downregulated probe sets between 10 DLBCL cell lines using a twofold expression change cut-off. **e**, Heat map showing the average gene expression intensities of the 35 probe sets exhibiting significantly increased expression in at least four of the five most sensitive mutant DLBCL cell lines (Pfeiffer, KARPAS-422, WSU-DLCL2, SU-DHL-10 and SU-DHL-6).

Toledo cells, a cell line with wild-type EZH2 whose growth is not affected by EZH2 inhibition (Fig. 3a). Even at $2\,\mu M$ GSK126, very few transcriptional changes were observed in Toledo cells (23 upregulated and 10 downregulated probe sets), despite a near complete loss of H3K27me3 at this dose and time (Supplementary Table 6 and Supplementary Fig. 3c). Likewise, quantitative PCR with reverse transcription (qRT–PCR) performed for quantitative mRNA expression analysis of two H3K27me3-enriched genes revealed dose-responsive increases in gene expression with as little as 25 nM GSK126 in Pfeiffer and KARPAS-422 cells, but no transcriptional changes in Toledo cells with up to $1\,\mu M$ GSK126 (Fig. 3c and Supplementary Table 7). Interestingly, even in the most sensitive wild-type EZH2 cell line, HT, the transcriptional response was less pronounced when compared to EZH2 mutant DLBCL cell lines with similar sensitivity (Fig. 3a). Relaxing the transcriptional fold-change criteria from 2.0 to 1.5 revealed additional modest transcriptional changes in HT cells (Supplementary Fig. 8b). This muted transcriptional response in wild-type EZH2 and less sensitive mutant cell lines indicates that other compensatory mechanisms (such as H3K9, H4K20 or DNA methylation) may exist in these cell lines to dampen the transcriptional response.

Among the EZH2 mutant cell lines, global H3K27me3 levels were statistically higher in transcriptionally responsive lines (t-test, $P = 0.019$), indicating that EZH2 mutation status together with global H3K27me3 levels may be a better predictive biomarker than mutation status alone (Supplementary Fig. 8c). Whereas the five most sensitive EZH2 mutant cell lines showed a preponderance of upregulated gene expression changes (69–95%), little overlap was observed among the differentially regulated probe sets using either twofold or 1.5-fold significance criteria (Fig. 3d and Supplementary Fig. 8d). Only 35 upregulated probe sets were common to at least four of these five mutant cell lines (Supplementary Table 8). Examination of these commonly upregulated probe sets revealed that many are enriched for H3K27me3 (32/35) (Supplementary Tables 7 and 8). Additionally, many of these probe sets are induced, albeit weakly, in the other cell lines, indicating that additional time or chromatin factors may be required for complete gene activation in these settings (Fig. 3e and Supplementary Table 8). Lastly, whereas no single pathway or process was significantly enriched among the limited set of genes commonly upregulated, gene ontology enrichment analysis of regulated gene sets in each cell line individually revealed several common processes including cell cycle regulation, cell death and regulation of biological/cellular processes (Supplementary Fig. 12 and Supplementary Table 9). These data demonstrate that the global loss of H3K27me3 following inhibition of EZH2 with GSK126 is associated with transcriptional activation of EZH2 target genes that correlates well with sensitivity, and that mutant EZH2 de-regulates H3K27me3 in a global, rather than targeted, manner. The significant variation between the upregulated gene sets of sensitive cell lines is a surprising observation that likely highlights the complexity and uniqueness of the epigenome in each cell line, and the diversity of selective pressures during the development of individual lymphomas.

On the basis of its potent effects in cell culture, we evaluated GSK126 in mice using subcutaneous xenografts of KARPAS-422 and Pfeiffer cells. Following 10 days of once-daily dosing of GSK126, global H3K27me3 decreased and gene expression increased in a dose-dependent fashion consistent with observations from cell culture (Fig. 4a, b). Although GSK126 was initially cleared rapidly from the blood, there was an extended terminal phase where drug elimination from blood and tumour was slower (Supplementary Fig. 13a, b). With daily 50 mg per kg dosing, complete tumour growth inhibition was observed in both KARPAS-422 and Pfeiffer cell models (Fig. 4c and Supplementary Fig. 14a). When higher dosing regimens were examined with KARPAS-422 xenografts, marked tumour regression was observed (Fig. 4c). Upon cessation of dosing, tumours in the 50 mg per kg once daily group showed tumour stasis whereas complete tumour eradication was observed in the 150 mg per kg once daily and 300 mg per kg twice per week groups. Tumour growth inhibition
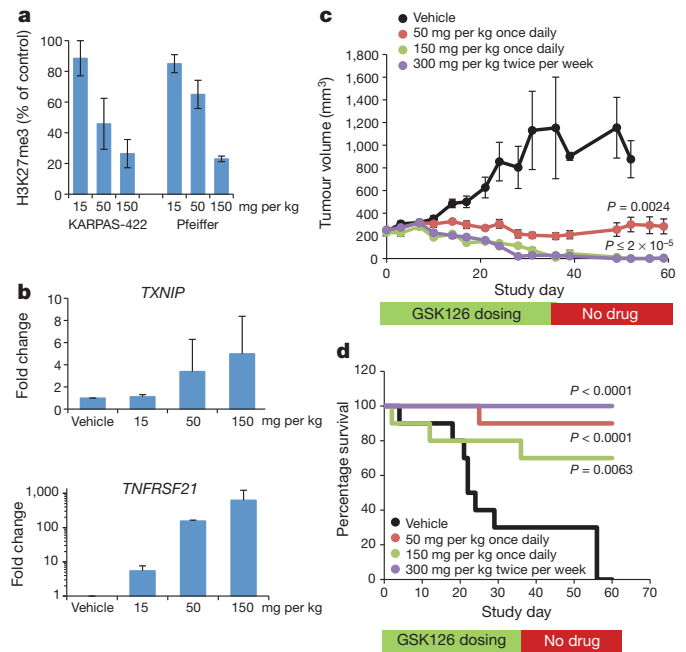
Figure 4 | *In vivo* inhibition of H3K27me3 and tumour growth response with GSK126. a, Response of H3K27me3 in tumour xenografts following 10 days of once daily dosing with GSK126. b, qRT–PCR analysis of EZH2 target genes in KARPAS-422 tumour xenografts. Mean values ± s.d. ($n = 3$) are shown (a, b). c, Activity of GSK126 on the growth of subcutaneous KARPAS-422 xenografts. Mean tumour volume ± s.e.m. is shown ($n = 10$). d, Kaplan–Meier survival curve of mice treated in c. Significant P values, calculated using a nonparametric log-rank test, between vehicle and treatment groups are indicated. No significant differences were observed between treatment groups (P values = 0.07–0.32).

also correlated with statistically significant increased survival of mice bearing the more aggressive KARPAS-422 tumours, where spontaneous deaths occurred in vehicle-treated animals (Fig. 4d). On the basis of these striking observations, intermittent dosing regimens with lower doses of GSK126 given weekly or with a 1 week drug holiday were examined in KARPAS-422 tumour xenografts with large tumours (Supplementary Fig. 14b). All schedules demonstrated tumour growth inhibition (91–100%, t-test, P values = 0.0008–0.0024). These results indicate that the response to GSK126 is durable and that intermittent dosing schedules may be effective in a clinical setting even in advanced tumours.

GSK126 was well tolerated at the doses and schedules examined as measured by little to no decrease in body weight, normal grooming and behaviour, and vastly improved survival in mice carrying KARPAS-422 xenografts (Supplementary Fig. 15a–c and Fig. 4d). Given the role of EZH2 in normal haematopoiesis and the identification of EZH2 loss-of-function mutations in myeloid malignancies[20–23], we investigated the effects of GSK126 treatment on peripheral blood of immunocompetent mice. Complete blood count analysis revealed no significant changes in any blood cell types at doses and times where efficacy was observed in tumour xenografts (Supplementary Fig. 15d).

Over the past decade, the development of targeted agents that specifically inhibit oncoproteins with activating somatic alterations has provided profound clinical benefit for cancer patients[24,25]. The data shown here provide compelling evidence that inhibition of EZH2 methyltransferase activity may be a viable strategy for the treatment of DLBCL and non-indolent follicular lymphoma harbouring activating mutations in EZH2. GSK126 also provides a means to evaluate whether EZH2 activity is required for the survival of tumours where EZH2 overexpression has been linked to poor prognosis[2–5], and tumours harbouring loss-of-function mutations in UTX[17,21,26].

Although we do not expect GSK126 to be effective in treating myeloid malignancies bearing loss-of-function mutations in EZH2 (refs 21–23), GSK126 should be an important tool to assess the role of EZH2 in normal myeloid development and to understand the oncogenic role of EZH2 in myeloproliferative neoplasms. Lastly, the identification of a selective EZH2 inhibitor which does not lead to degradation of the PRC2 complex provides a useful tool to understand the role of EZH2 methyltransferase activity versus its scaffolding role in development, tumorigenesis and tumour progression that could not be elucidated through conventional genetic manipulation studies.

METHODS SUMMARY

Biochemical assays used the five-member PRC2 complex (human Flag–EZH2, EED, SUZ12, AEBP2, RbAp48) containing either wild-type or mutant EZH2, [^{3}H]-SAM and the indicated peptide substrate; reactions were incubated for 30 min. Global histone modification levels were determined by enzyme-linked immunosorbent assay (ELISA) or western blot methods using antibodies specific for total histone H3, H3K27me1, H3K27me2 or H3K27me3. Cell proliferation and caspase-3/7 activity were assessed using CellTiter-Glo and Caspase-Glo 3/7 (Promega), respectively. Gene expression profiling was conducted using Affymetrix Human Genome U133 Plus 2.0 microarrays. Differentially expressed probe sets were determined by fitting the data to a linear model using the limma statistical package (http://www.bioconductor.org) and carrying out pair-wise contrasts of treated versus control. Significant probe sets were filtered for detection ($\log_2$ signal threshold of 8), an average fold-change >2 or <-2, or >1.5 or <-1.5, where indicated, with P values adjusted for multiple testing correction by false discovery rate (FDR; Benjamini–Hochberg) < 0.1. H3K27me3 ChIP reads were aligned using Bowtie[27]. H3K27me3 enrichment peaks were identified using SICER[28] with optimized parameters. A custom PERL script was used to quantify the average basal H3K27me3 ChIP-seq tag density across gene sets. All *in vivo* studies were conducted after review by the Institutional Animal Care and Use Committee at GSK and in accordance with the GSK Policy on the Care, Welfare and Treatment of Laboratory Animals. GSK126 and vehicle were administered to mice intraperitoneally. Two-tailed *t*-tests were conducted assuming two samples of equal variance. A complete description of the materials and methods is provided in Supplementary Information.

Full Methods and any associated references are available in the online version of the paper.

1. Varambally, S. *et al.* Genomic loss of microRNA-101 leads to overexpression of histone methyltransferase EZH2 in cancer. *Science* **322,** 1695–1699 (2008).
2. Varambally, S. *et al.* The polycomb group protein EZH2 is involved in progression of prostate cancer. *Nature* **419,** 624–629 (2002).
3. Kleer, C. G. *et al.* EZH2 is a marker of aggressive breast cancer and promotes neoplastic transformation of breast epithelial cells. *Proc. Natl Acad. Sci. USA* **100,** 11606–11611 (2003).
4. Wagener, N. *et al.* Enhancer of zeste homolog 2 (EZH2) expression is an independent prognostic factor in renal cell carcinoma. *BMC Cancer* **10,** 524 (2010).
5. Takawa, M. *et al.* Validation of the histone methyltransferase EZH2 as a therapeutic target for various types of human cancer and as a prognostic marker. *Cancer Sci.* **102,** 1298–1305 (2011).
6. Morin, R. D. *et al.* Frequent mutation of histone-modifying genes in non-Hodgkin lymphoma. *Nature* **476,** 298–303 (2011).
7. Morin, R. D. *et al.* Somatic mutations altering EZH2 (Tyr641) in follicular and diffuse large B-cell lymphomas of germinal-center origin. *Nature Genet.* **42,** 181–185 (2010).
8. Pasqualucci, L. *et al.* Analysis of the coding genome of diffuse large B-cell lymphoma. *Nature Genet.* **43,** 830–837 (2011).
9. McCabe, M. T. *et al.* Mutation of A677 in histone methyltransferase EZH2 in human B-cell lymphoma promotes hypertrimethylation of histone H3 on lysine 27 (H3K27). *Proc. Natl Acad. Sci. USA* **109,** 2989–2994 (2012).
10. Ryan, R. J. *et al.* EZH2 codon 641 mutations are common in BCL2-rearranged germinal center B cell lymphomas. *PLoS ONE* **6,** e28585 (2011).
11. Sneeringer, C. J. *et al.* Coordinated activities of wild-type plus mutant EZH2 drive tumor-associated hypertrimethylation of lysine 27 on histone H3 (H3K27) in human B-cell lymphomas. *Proc. Natl Acad. Sci. USA* **107,** 20980–20985 (2010).
12. Wigle, T. J. *et al.* The Y641C mutation of EZH2 alters substrate specificity for histone H3 lysine 27 methylation states. *FEBS Lett.* **585,** 3011–3014 (2011).
13. Yap, D. B. *et al.* Somatic mutations at EZH2 Y641 act dominantly through a mechanism of selectively altered PRC2 catalytic activity, to increase H3K27 trimethylation. *Blood* **117,** 2451–2459 (2011).
14. Diaz, E. *et al.* Development and validation of reagents and assays for EZH2 peptide and nucleosome high-throughput screens. http://dx.doi.org/10.1177/1087057112453765 *J. Biomol. Screen.* (2012).
15. Schubert, H. L., Blumenthal, R. M. & Cheng, X. Many paths to methyltransfer: a chronicle of convergence. *Trends Biochem. Sci.* **28,** 329–335 (2003).
16. Miranda, T. B. *et al.* DZNep is a global histone methylation inhibitor that reactivates developmental genes not silenced by DNA methylation. *Mol. Cancer Ther.* **8,** 1579–1588 (2009).
17. van Haaften, G. *et al.* Somatic mutations of the histone H3K27 demethylase gene *UTX* in human cancer. *Nature Genet.* **41,** 521–523 (2009).
18. Dyer, M. J., Fischer, P., Nacheva, E., Labastide, W. & Karpas, A. A new human B-cell non-Hodgkin's lymphoma cell line (Karpas 422) exhibiting both t(14;18) and t(4;11) chromosomal translocations. *Blood* **75,** 709–714 (1990).
19. Al-Katib, A. M. *et al.* Bryostatin 1 down-regulates *mdr1* and potentiates vincristine cytotoxicity in diffuse large cell lymphoma xenografts. *Clin. Cancer Res.* **4,** 1305–1314 (1998).
20. Chou, R. H., Yu, Y. L. & Hung, M. C. The roles of EZH2 in cell lineage commitment. *Am. J. Transl. Res.* **3,** 243–250 (2011).
21. Jankowska, A. M. *et al.* Mutational spectrum analysis of chronic myelomonocytic leukemia includes genes associated with epigenetic regulation: *UTX, EZH2,* and *DNMT3A. Blood* **118,** 3932–3941 (2011).
22. Ernst, T. *et al.* Inactivating mutations of the histone methyltransferase gene *EZH2* in myeloid disorders. *Nature Genet.* **42,** 722–726 (2010).
23. Makishima, H. *et al.* Novel homo- and hemizygous mutations in *EZH2* in myeloid malignancies. *Leukemia* **24,** 1799–1804 (2010).
24. Chapman, P. B. *et al.* Improved survival with vemurafenib in melanoma with BRAF V600E mutation. *N. Engl. J. Med.* **364,** 2507–2516 (2011).
25. Kwak, E. L. *et al.* Anaplastic lymphoma kinase inhibition in non-small-cell lung cancer. *N. Engl. J. Med.* **363,** 1693–1703 (2010).
26. Gui, Y. *et al.* Frequent mutations of chromatin remodeling genes in transitional cell carcinoma of the bladder. *Nature Genet.* **43,** 875–878 (2011).
27. Langmead, B., Trapnell, C., Pop, M. & Salzberg, S. L. Ultrafast and memory-efficient alignment of short DNA sequences to the human genome. *Genome Biol.* **10,** R25 (2009).
28. Zang, C. *et al.* A clustering approach for identification of enriched domains from histone modification ChIP-Seq data. *Bioinformatics* **25,** 1952–1958 (2009).

METHODS

Determination of K_i^{app} values for GSK126 inhibition of wild-type and mutant EZH2. The five-member PRC2 complex (Flag–EZH2, EED, SUZ12, AEBP2, RbAp48) containing either wild-type or mutant (A677G, Y641N, Y641C, Y641H, Y641S or Y641F) EZH2 was prepared as previously described[9]. GSK126 was dissolved in DMSO and tested at concentrations of 0.6 nM to 300 nM with a final DMSO concentration of 2.5%. In contrast to wild-type EZH2 which prefers H3K27me0 as a substrate *in vitro*, EZH2 Y641 mutants prefer H3K27me2 and have little activity with H3K27me0 or H3K27me1. The A677G mutant is distinct from both the wild-type and Y641 mutant forms of EZH2 in that it efficiently methylates H3K27me0, H3K27me1, and H3K27me2; therefore, histone H3 peptides (residues 21–44; 10 μM final) with either K27me0 (wild type, A677G EZH2), K27me1 (A677G EZH2), or K27me2 (A677G, Y641N, Y641C, Y641H, Y641S and Y641F EZH2) were used as methyltransferase substrates. GSK126 was added to plates followed by addition of 6 nM EZH2 complex and peptide. As the potency of GSK126 is at or near the tight binding limit of an assay run at $[SAM] = K_m$, we used a method where IC$_{50}$ values were measured at a high concentration of the competitive substrate SAM relative to its K_m (7.5 μM SAM where the SAM K_m is 0.3 μM). Under these conditions, the contribution from the enzyme concentration becomes relatively small (see equation (1)) and accurate estimates of K_i can be calculated[29]. Reactions were initiated with [^{3}H]-SAM, incubated for 30 min, quenched with the addition of 500-fold excess unlabelled SAM, and the methylated product peptide was captured on phosphocellulose filters according to the vendor supplied protocol for MSPH Multiscreen plates (EMD Millipore). Plates were read on a TopCount after adding 20 μl of Microscint-20 cocktail (both from PerkinElmer). Apparent K_i values ± s.d. were calculated using the Cheng–Prusoff relationship[30] for a competitive inhibitor ($n = 2$).

$$IC_{50} = K_i(1 + [S]/K_m) + [E]/2 \qquad (1)$$

where E is the enzyme and S is the substrate.

Mechanism of GSK126 inhibition of EZH2. IC$_{50}$ values were determined for GSK126 inhibition of EZH2 at several SAM concentrations ranging from 0.9 μM to 15 μM and then separately at several peptide concentrations ranging from 16 μM to 60 μM using the assay conditions described above. The resulting IC$_{50}$ values were plotted against the $[SAM]/K_m$ ratio or the $[peptide]/K_m$ ratio, respectively.

Cell culture and immunoblotting. Cell lines were obtained from the American Type Culture Collection or the Deutsche Sammlung von Mikroorganismen und Zellbulturen and maintained in the recommended cell culture media at 37 °C in 5% CO$_2$. Cells were lysed with radioimmunoprecipitation (RIPA) buffer (Thermo Scientific) and western blot analysis was conducted as previously described[9]. Antibodies were obtained as previously described[9] or from Cell Signaling Technology (SUZ12, 3737), or Santa Cruz Biotechnology (EED, sc-28701).

H3K27 methylation status and PRC2 components following GSK126 treatment. Cells (2×10^5 per well) were seeded into six-well tissue culture plates in the appropriate cell culture media 24 h before treatment. Cells were then exposed to 0.1% DMSO or varying concentrations of GSK126 (range = 25 nM–2 μM) for 24, 72 or 144 h.

Enzyme-linked immunosorbent assay (ELISA)-based quantification of total histone H3 and H3K27me3 levels. Following tissue homogenization, tumour tissue lysates were prepared using the Epigentek Histone Extraction kit (OP-0006). Alternatively, cells were seeded at 2,000 cells per well in a 96-well plate and were treated with a 10-point threefold dilution series of GSK126 (dose range = 2 nM–38 μM) for 48 h. Cells were lysed with 0.2 N HCl for 30 min to extract histones, the acid-insoluble portion was pelleted by centrifugation, and the supernatant was neutralized with neutralization buffer (1 M Na$_2$HPO$_4$, pH 12.5; ActiveMotif) containing protease inhibitors (Roche). Lysates were added to Maxisorp ELISA plates (Nunc) in duplicate on each of two plates plus blocking buffer (1% BSA). Plates were incubated for 1 h, washed four times with imidazole buffered saline containing Tween-20 (Kirkegaard & Perry Laboratories), incubated with primary antibodies for H3K27me3 or total H3, washed, incubated with horseradish peroxidase (HRP)-linked secondary anti-rabbit IgG antibody, and washed again. Luminata Forte substrate (Millipore) was added 5 min before chemiluminescence was quantified with an EnVision multi-label plate reader (PerkinElmer). H3K27me3 levels were normalized to total H3 values and IC$_{50}$ values were determined using a four-parameter curve fit.

Cell proliferation assay. The optimal cell seeding was determined empirically for all cell lines by examining the growth of a wide range of seeding densities in a 384-well format to identify conditions that permitted proliferation for 6 days. Cells were then plated at the optimal seeding density 24 h before treatment (in duplicate) with a 20-point twofold dilution series of GSK126 or 0.15% DMSO. Plates were incubated for 6 days at 37 °C in 5% CO$_2$. Cells were then lysed with

CellTiter-Glo (CTG) (Promega) and chemiluminescent signal was detected with a TECAN Safire2 microplate reader. In addition, an untreated plate of cells was harvested at the time of compound addition (T$_0$) to quantify the starting number of cells. CTG values obtained after the 6 day treatment were expressed as a percent of the T$_0$ value and plotted against compound concentration. Data were fit with a four-parameter equation to generate a concentration response curve and the concentration of GSK126 required to inhibit 50% of growth (growth IC$_{50}$) was determined.

Caspase 3/7 assay. For detection of caspase-3/7 activity, cells were cultured in 96-well plates, treated with a 10-point threefold dilution series of GSK126 (range 0.03 nM to 5 μM) and evaluated using Caspase-Glo 3/7 (Promega) as per the manufacturer's instructions. Values were normalized to CTG (Promega) levels at each time point and expressed as a percentage of vehicle treated control. Data represent an average of $n = 4$.

Cell cycle analysis. Cell cycle phase distribution was examined by flow cytometry. Twenty-four hours after seeding cells in a six-well culture plate, cells were treated with GSK126 or 0.1% DMSO (vehicle) for 3 days. Cells were washed with PBS, pelleted in CycleTest solution B (BD Biosciences, catalogue no. 340242b), flash frozen, and stored at −80 °C. CycleTest PLUS DNA reagent kit (BD Biosciences, catalogue no. 340242) was used according to the manufacturer's instructions to prepare and stain nuclei with propidium iodide. Samples were evaluated using a FACSCalibur flow cytometer (BD Biosciences) and data were analysed using FlowJo software (Tree Star).

Gene expression profiling. Cells (2×10^5 per well) were seeded into six-well tissue culture plates in the appropriate cell culture media 24 h before treatment. Duplicate wells were then exposed to 0.1% DMSO, 500 nM or 2 μM GSK126 for 72 h. Cells were collected into TRIzol reagent (Invitrogen) and total RNA was isolated via phenol:chloroform extraction and the RNeasy kit (Qiagen) according to the manufacturer's instructions. Total RNA was labelled and hybridized to Affymetrix Human Genome U133 Plus 2.0 oligonucleotide microarrays arrays according to the manufacturer's instructions (Affymetrix) at Expression Analysis, Inc. These data are accessible through GEO via accession number GSE40972. Principal component and correlation analysis were used to confirm data reproducibility (Supplementary Fig. 16).

Affymetrix gene chip data analysis. CEL files, corresponding to individual samples, were processed by the Micro Array Suite 5.0 (MAS5) algorithm (http://www.affymetrix.com/support/index.affx) where signal values were scaled to a target intensity of 500 and log$_2$ transformed. Differentially expressed probe sets were determined by fitting the data to a linear model and carrying out pairwise contrasts of treated versus control. Significant probe sets were filtered for detection (log$_2$ signal threshold of 8), an average fold-change >2 or <-2, or >1.5 or <-1.5, where indicated, with P-values adjusted for multiple testing correction by false discovery rate (FDR) (Benjamini–Hochberg) < 0.1. Statistical analyses were performed using the limma package from Bioconductor (http://www.bioconductor.org/). Functional analyses of differentially expressed probe sets were performed using DAVID (http://david.abcc.ncifcrf.gov/). Significantly over-represented GO Biological Process and Molecular Function terms (levels 3–5) were filtered for EASE P-value < 0.01.

qRT–PCR. Cells were treated for 72 h with 0.1% DMSO or a range of concentrations of GSK126 (range = 25 nM–1 μM) and total RNA was isolated as described above. RNA (2.8 μg) was reverse transcribed with MultiScribe Reverse Transcriptase (Applied BioSystems) according to the manufacturer's recommendations. The resulting cDNA was diluted and used along with TaqMan gene expression assays (Applied Biosystems; *GAPDH*, Hs03929097_g1; *TNFRSF21*, Hs00205419_m1; *TXNIP*, Hs00197750_m1). TaqMan Gene Expression Master Mix (Applied BioSystems) and a ViiA 7 Real-Time PCR System (Applied BioSystems) were used according to the manufacturer's recommendations to quantify gene expression.

ChIP-seq. Cells (5×10^7) were maintained in the appropriate cell culture media for 24 h before fixation. Cells were fixed for 15 min at room temperature with freshly prepared formaldehyde solution (final concentrations 1% formaldehyde, 10 mM NaCl, 0.1 mM EDTA pH 8.0, 5 mM HEPES pH 7.9) followed by the addition of glycine to 125 mM. Fixed cells were rinsed twice in PBS containing 0.5% Igepal CA-630 (Sigma) and cell pellets were flash frozen. ChIP assays were performed using a custom assay protocol at Active Motif Inc. H3K27me3 ChIP and input libraries were prepared for 35 nucleotide single-end sequencing on an Illumina GAIIx sequencer according to manufacturer's instructions. These data are accessible through GEO via accession number GSE40970. Reads were assessed for quality (base quality <20 were excluded) and aligned to human reference sequence (hg19 build) using the Bowtie[27] algorithm allowing for up to two mismatches. Only uniquely mapped reads were used for subsequent analyses.

ChIP-seq analysis. The average basal H3K27me3 ChIP-seq tag count was quantified across genes that were upregulated, downregulated or unchanged following

treatment with GSK126 using a custom PERL script. In addition to the gene body, a region encompassing 10 kilobases (kb) upstream of the transcription initiation site and 10 kb downstream of the transcription termination site were evaluated. All genes were oriented by strand, and the variable length of gene bodies were standardized to 10,000 bins. After averaging the numbers of sequence tags at each base pair the values were normalized to the total number of mapped sequence tags per ChIP. A 500 base pair (bp) centred moving average was then applied to highlight larger trends and smooth out short-range fluctuations. MultiExperiment Viewer (http://www.tm4.org/mev/) was used to evaluate enrichment across individual genes. Peaks of H3K27me3 enrichment were identified using the peak calling software SICER[28] with the following parameters: fragment size, 250 bp; effective genome size fraction, 0.86; window size, 750 bp; gap size, 3; redundancy threshold, 1; FDR, 0.001. Statistically significant peaks (FDR < 0.001) enriched in the ChIP sample relative to its corresponding input sample were annotated for genomic location and were assigned to genes within ±10 kb from transcription start site (TSS) to identify target genes: upstream (−10 to 2.5 kb relative to TSS), promoter (−2.5 kb to +2.5 kb), 5′UTR, coding region, 3′UTR. All genes were considered in the 5′→3′ orientation. Bedtools was used for manipulation and analysis of data and IGV (http://www.broadinstitute.org/igv/) was used for visualization. Annotation files were downloaded from UCSC.

RNA isolation from tumour xenografts. QIAzol (300 μl per mg tumour) (Qiagen) was added to tumour xenograft tissue. The tumour was lysed and homogenized using the Qiagen TissueLyzer and stainless steel beads. Chloroform was added to the QIAzol lysate. The QIAzol/chloroform homogenate was then added to a Qiagen MaXtract High Density tube (Qiagen). The aqueous phase was transferred to a fresh tube and mixed with an equal volume of 70% ethanol and applied to a Qiagen RNeasy column (Qiagen). The remaining RNA isolation was carried out according to the manufacturer's protocol.

In vivo **studies.** All studies were conducted after review by the Institutional Animal Care and Use Committee at GSK and in accordance with the GSK Policy on the Care, Welfare and Treatment of Laboratory Animals. For all *in vivo* studies, GSK126 or vehicle was administered intraperitoneally at a dose volume of 0.2 ml per 20 g body weight in 20% captisol adjusted to pH 4–4.5 with 1 N acetic acid. Pfeiffer or KARPAS-422 cells (1×10^7) in 100% Matrigel (BD Biosciences) were implanted subcutaneously in female beige SCID mice. Tumours were measured with calipers, and block randomized according to tumour size into treatment groups. For efficacy studies, 10 mice were randomized in each treatment group before the initiation of dosing and GSK126 treatment was initiated once the tumour volumes were approximately 200 mm^3 in the Pfeiffer and KARPAS-422 studies (Fig. 4c and Supplementary Fig. 14a) and 500 mm^3 in the KARPAS-422 intermittent dosing study (Supplementary Fig. 14b). Mice were weighed and tumours measured with calipers twice weekly. Two-tailed *t*-tests were conducted assuming two samples of equal variance. For mouse pharmacokinetic studies, tumour and blood samples were harvested from euthanized mice at the indicated time. Blood and tumour homogenates were flash frozen and subsequently analysed by HPLC/MS/MS to evaluate the concentration of GSK126. For pharmacodynamic studies, a portion of each tumour was frozen for H3K27me3/H3 ELISAs or placed in RNAlater (Ambion) for RNA isolation. For peripheral blood analyses, blood was harvested via cardiac puncture from euthanized, immunocompetent female CD-1 mice (three mice per group) on day 18. Blood was immediately placed into a Microtainer EDTA tube (BD) and gently mixed by inverting. A complete blood count analysis was conducted using the Advia 2120 haematology analyser (Siemens Medical Solutions) using multi-species software as per manufacturer's instructions.

29. Tornheim, K. Kinetic applications using high substrate and competitive inhibitor concentrations to determine K_i or K_m. *Anal. Biochem.* **221,** 53–56 (1994).
30. Yung-Chi, C. & Prusoff, W. H. Relationship between the inhibition constant (K_I) and the concentration of inhibitor which causes 50 per cent inhibition (I_{50}) of an enzymatic reaction. *Biochem. Pharmacol.* **22,** 3099–3108 (1973).

a

b
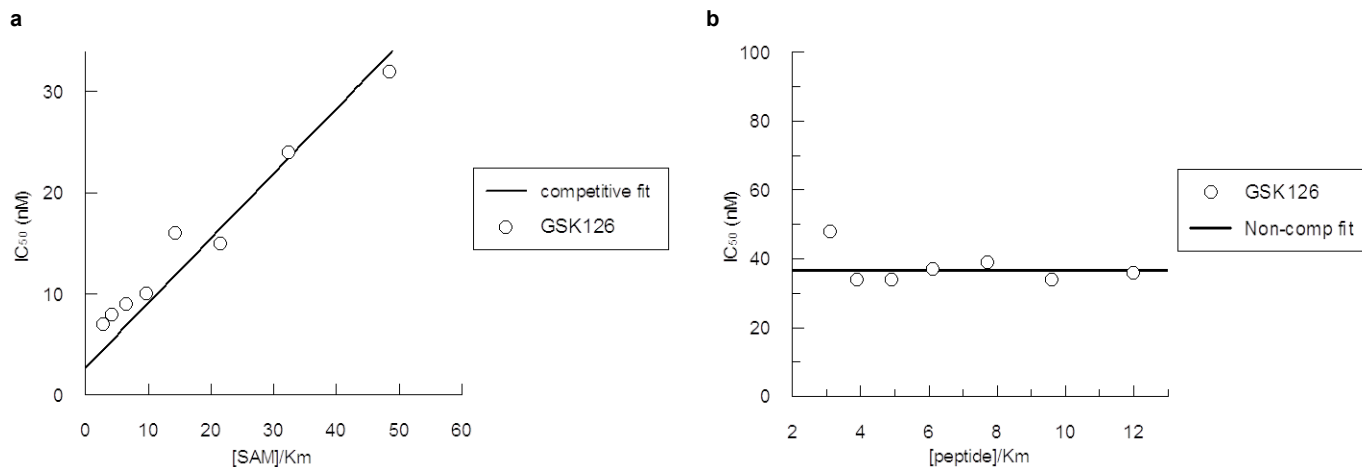
Supplementary Figure 1 | Mechanism of EZH2 inhibition. **a** The potency of GSK126 is near the concentration of EZH2 used in the assays; therefore, standard mechanism of inhibition determination through double titration of inhibitor and substrate followed by global fitting of the data is precluded. Instead, the IC_{50} values of GSK126 determined at several SAM concentrations (0.9 μM - 15 μM) were plotted against the [SAM]/K_m ratio. The data were fit to models of competitive, uncompetitive, and non-competitive inhibition and were best fit by a competitive model as determined by F-test analysis. **b** A similar experiment was performed using the peptide substrate over a range of peptide concentrations (16 μM - 60 μM). The inhibitor mechanism using peptide is best fit to a non-competitive model as determined by F-test analysis.
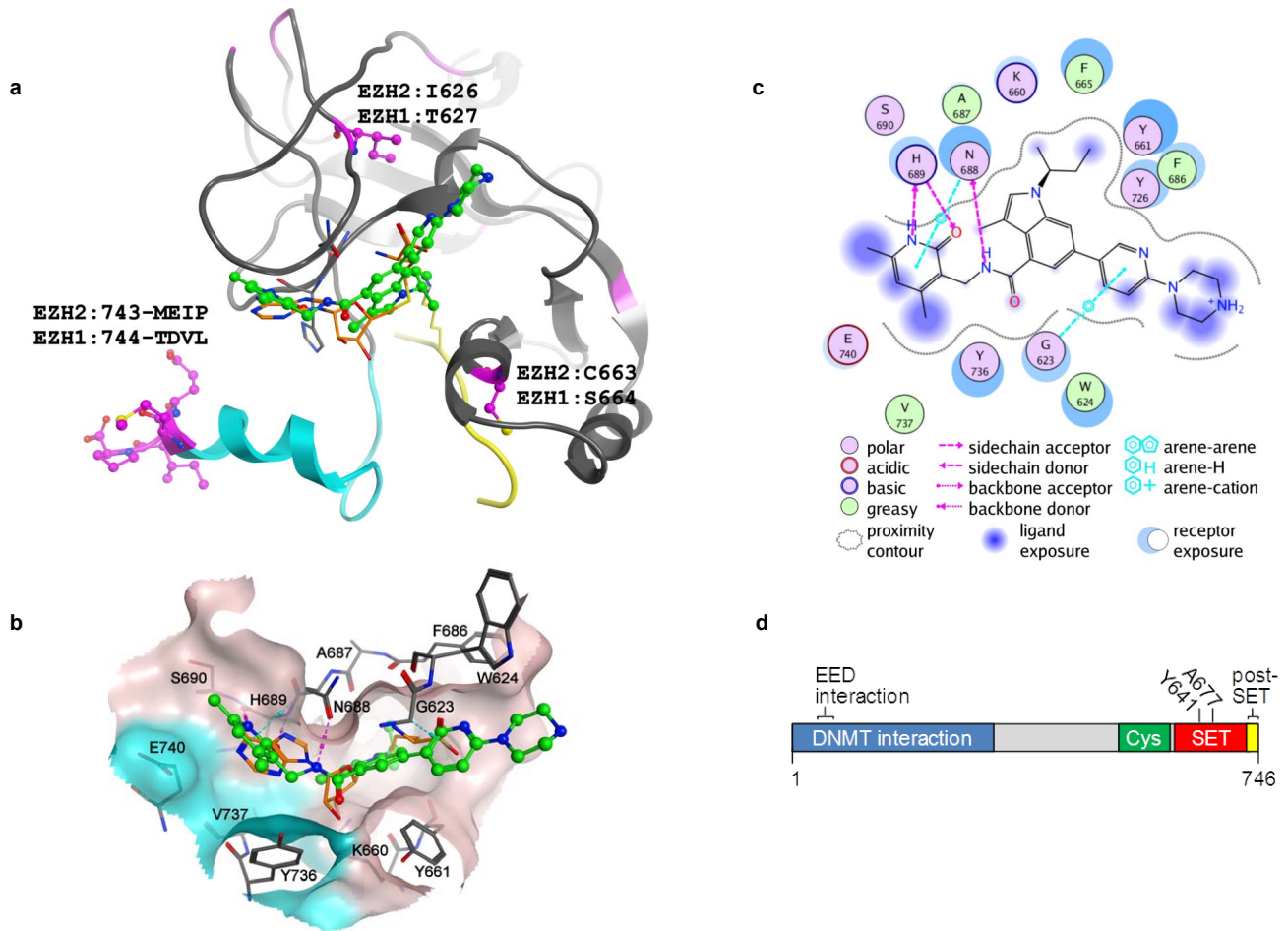
Supplementary Figure 2 | Homology model of EZH2 and predicted binding mode of GSK126. **a** A homology model of EZH2 and predicted binding mode of GSK126. GSK126 (green carbons) bound in the SAM binding site is overlaid with SAH (orange carbons). The H3K27me2 peptide substrate (yellow), the SET domain (grey ribbon) and the post-SET domain (cyan ribbon) and the residue differences between EZH2 and EZH1 within 10 Å of the predicted binding mode of GSK126 (magenta) are indicated. **b** A zoomed in view of the binding mode of GSK126 is depicted. Specific hydrogen bond and arene-H interactions are represented as dashed magenta and cyan lines, respectively. The binding site surface contributed by residues from the post-SET domain is colored cyan. **c** A 2D ligand interaction diagram highlighting specific interactions between residues of EZH2 and GSK126. **d** Diagram of EZH2 functional domains (UniProt Q15910) with the position of the A677 and Y641 activating mutations highlighted within the SET domain.
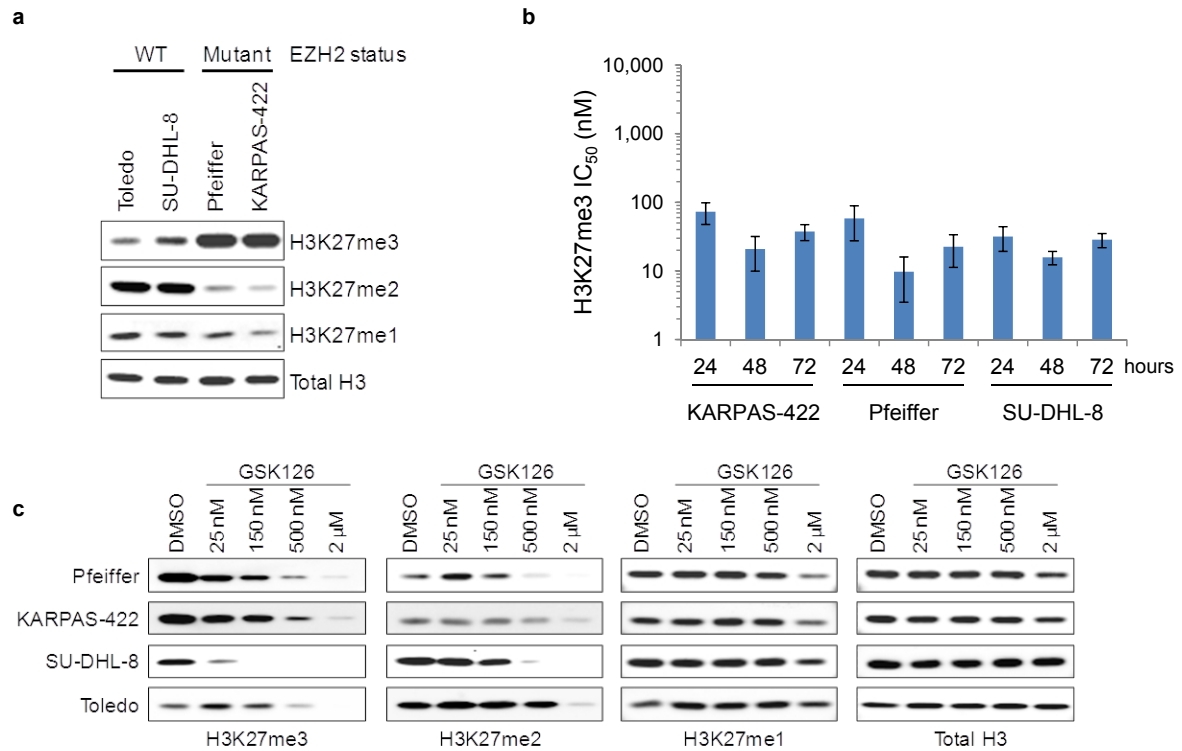
Supplementary Figure 3 | Analysis of H3K27 methylation in cell lines treated with GSK126. **a** Comparison of global H3K27me3, H3K27me2, and H3K27me1 levels across EZH2 WT (Toledo and SU-DHL-8) and mutant (Pfeiffer and KARPAS-422) lymphoma cell lines. **b** Potency of GSK126 over time as measured by reduction of global H3K27me3 levels in KARPAS-422, Pfeiffer, and SU-DHL-8 B-cell lymphoma cell lines. Cells were treated with a 3-fold dilution series of GSK126. The concentration of GSK126 required to reduce H3K27me3 levels by 50% (H3K27me3 IC_{50}) was determined by ELISA (n≥2; mean values ± s.d. are shown). **c** Evaluation of H3K27me3, H3K27me2, and H3K27me1 following treatment for 72 hours. Total histone H3 is shown as a loading control.

a *Pfeiffer (A677G)*

b *KARPAS-422 (Y641N)*

c *SU-DHL-8 (WT)*

d *Toledo (WT)*
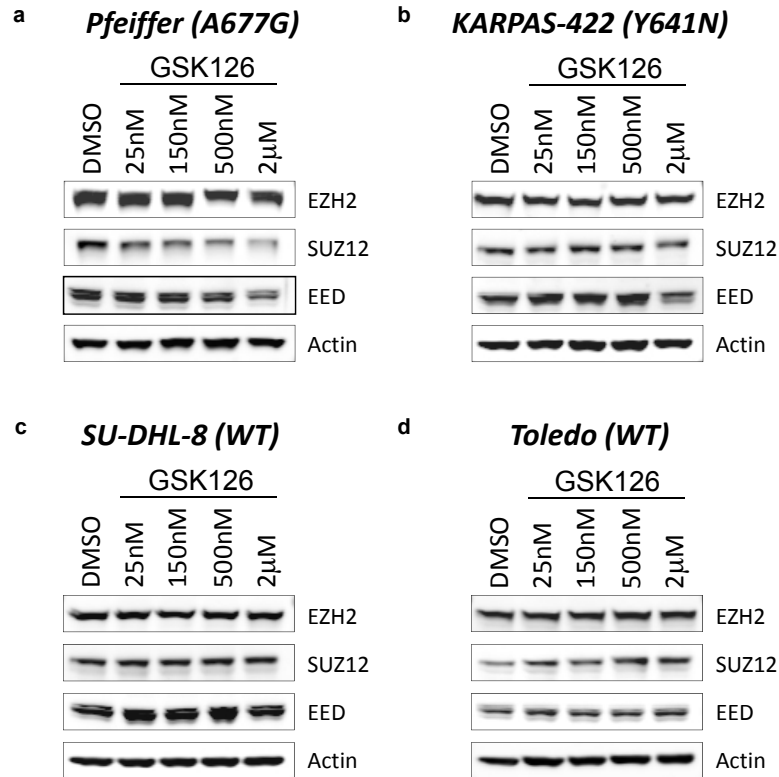
Supplementary Figure 4 | Western blot analysis of EZH2, SUZ12, and EED following treatment of EZH2 mutant (**a,b**) or WT (**c,d**) lymphoma cell lines with 0.1% DMSO (vehicle control), 25 nM, 150 nM, 500 nM, or 2 μM GSK126 for 72 hrs. Actin is included as a loading control.
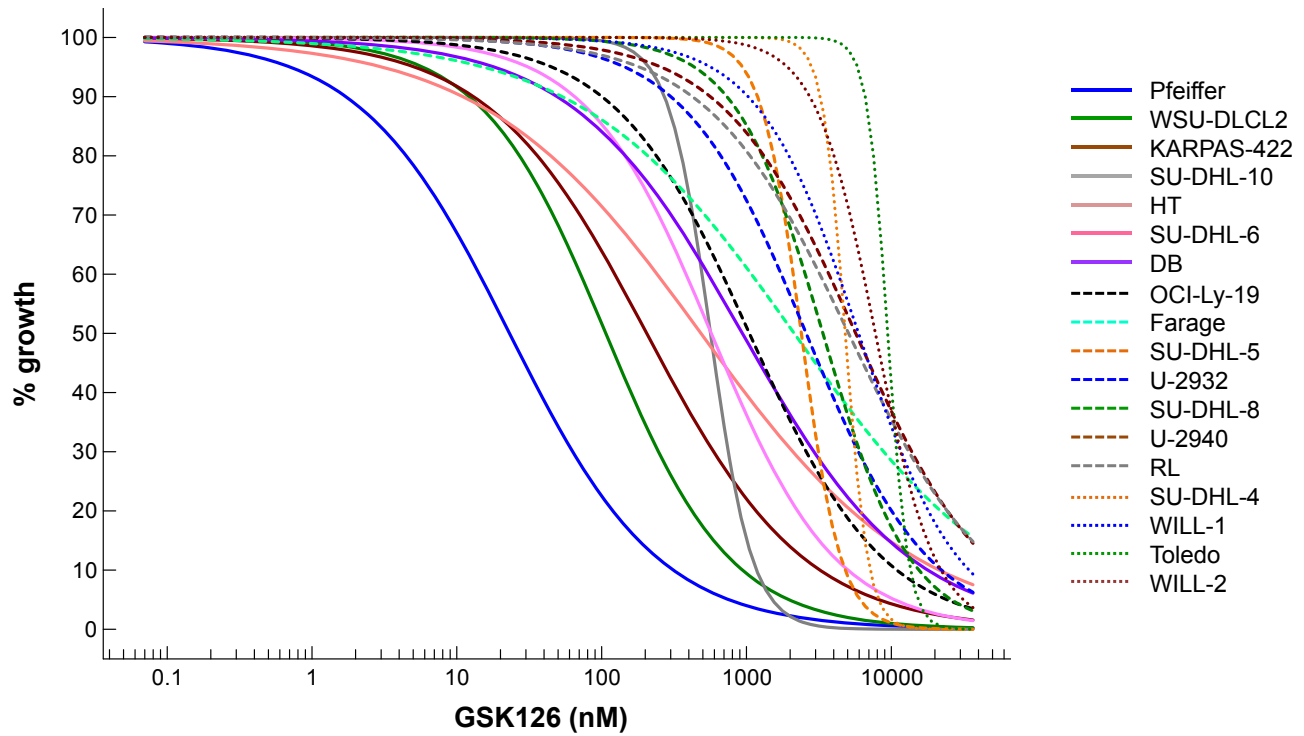
Supplementary Figure 5 | Composite dose-response curves demonstrating the effect of GSK126 on the growth of 18 DLBCL cell lines. Cell lines were treated with varying concentrations of GSK126 for 6 days before cell growth was evaluated with CellTiter-Glo (Promega). The y-axis represents the percent of growth relative to the vehicle control (0.15% DMSO).
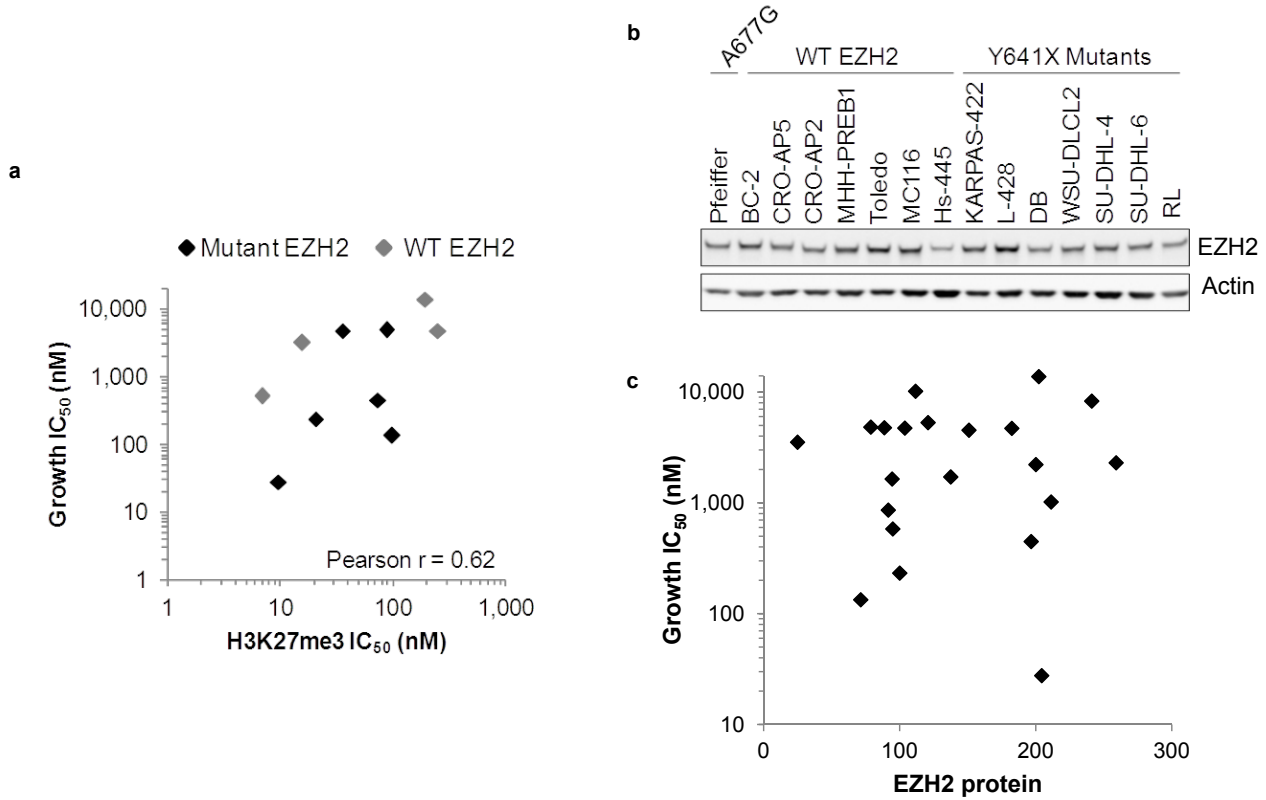
Supplementary Figure 6 | Correlation analysis between inhibition of H3K27me3, cell growth and EZH2 levels. **a** Cell growth IC_{50} values for GSK126 from Supplementary Table 5 plotted against H3K27me3 IC_{50} values for GSK126 from Figure 1c. Pearson correlation value is indicated. **b** A representative western blot of EZH2 and actin from whole cell extracts of lymphoma cell lines. Western blot signal intensities for EZH2 and actin were quantified using Li-Cor Odyssey software. **c** EZH2 signal intensities were normalized for total actin levels and plotted against cell growth IC_{50} values for GSK126 in a 6-day proliferation assay from Supplementary Table 5.
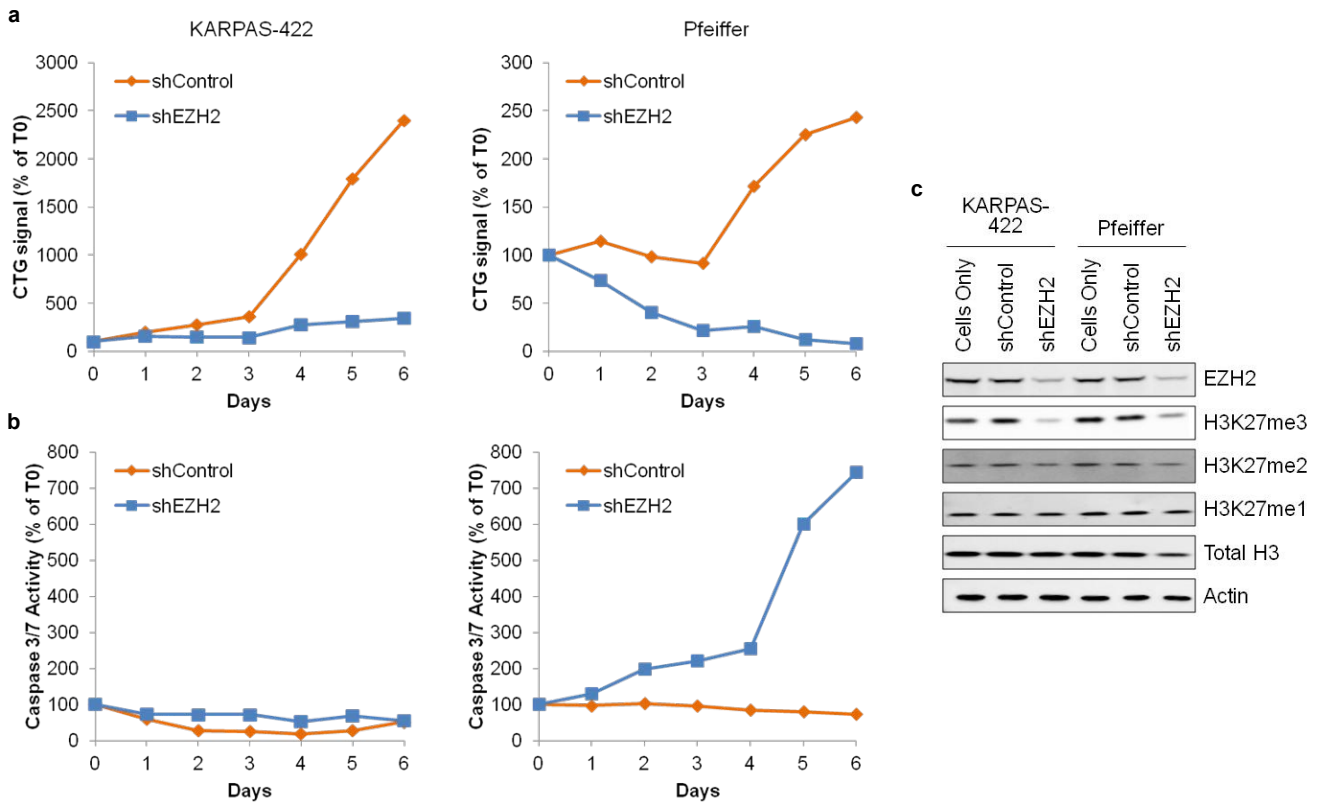
Supplementary Figure 7 | Phenotypic effects of EZH2 knockdown by shRNA. **a** Cell proliferation over a 6 day period for KARPAS-422 (left) and Pfeiffer (right) expressing an shRNA to EZH2 (blue) or a non-targeting control shRNA (orange). CTG signal at each time point is represented as a percentage of cells at day 0 (T_0). **b** Caspase 3/7 activity over time in KARPAS-422 (left) and Pfeiffer (right) expressing an shRNA to EZH2 (blue) or a non-targeting control shRNA (orange). Caspase 3/7 activity at each time point is represented as a percentage of activity at day 0 (T_0). **c** Western blot analysis of EZH2, H3K27me3, H3K27me2, H3K27me1, and total histone H3 following shRNA knockdown of EZH2. Actin is included as a loading control.

Supplementary Figure 8.
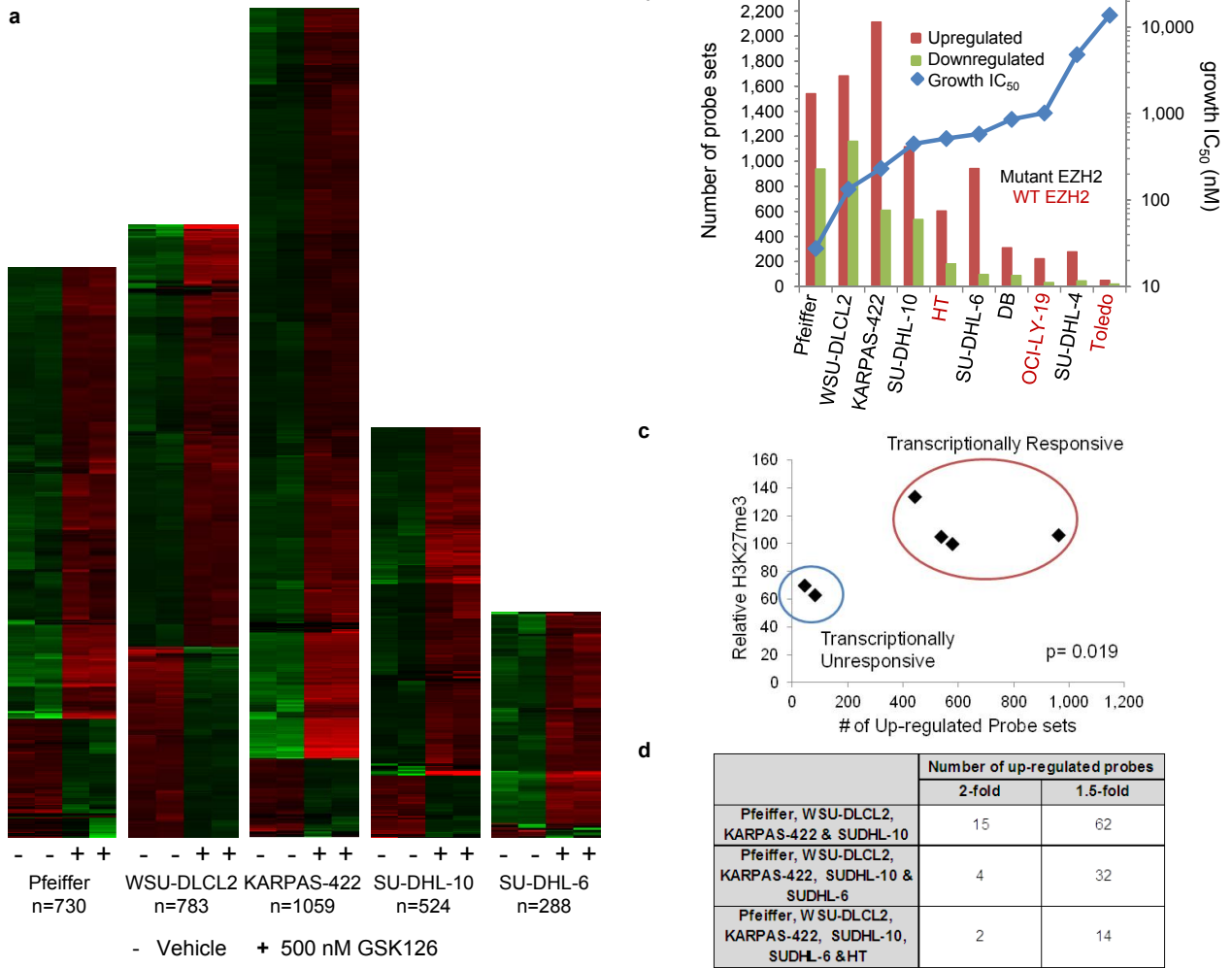
Supplementary Figure 8 | Expression analysis of DLBCL cell lines. **a** Gene expression heatmaps of normalized gene expression data for differentially expressed probe sets following treatment with GSK126 for 72 hours. Green, lower expression. Red, higher expression. **b** The number of probe sets exhibiting significantly altered gene expression (>1.5 or < -1.5 fold) following treatment of 10 DLBCL cell lines in duplicate for 72 hours with 500 nM GSK126 compared with 0.1% DMSO (vehicle control). **c** Correlation between the number of up-regulated probe sets and basal H3K27me3 levels in transcriptionally responsive and unresponsive mutant EZH2 DLBCL cell lines (Pfeiffer,WSU-DLCL2, KARPAS-422, SU-DHL-10, DB, and SU-DHL-4). H3K27me3 levels are normalized to total histone H3 and are expressed as a percentage of those levels observed in the Pfeiffer cell line. Transcriptionally responsive and unresponsive cell lines are circled in red and blue, respectively. **d** The number of common probe sets within indicated cell lines exhibiting a 1.5 or 2-fold increase in expression with GSK126 treatment.
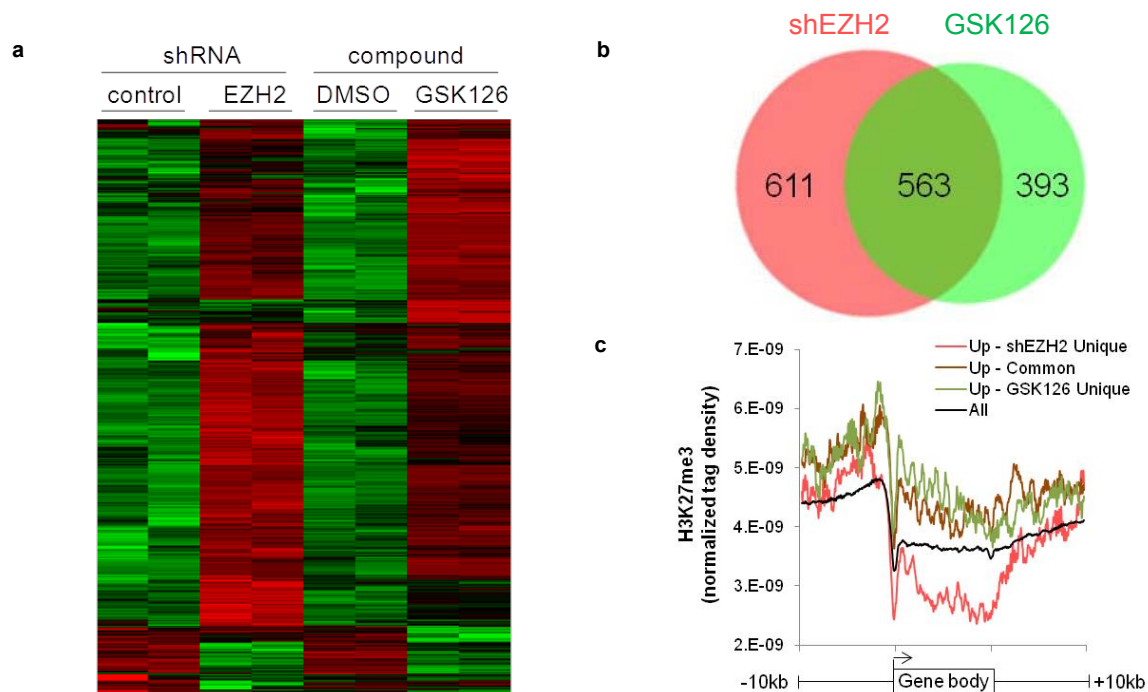
Supplementary Figure 9 | Comparison of gene expression changes elicited by EZH2 knockdown versus treatment with GSK126 in KARPAS-422. **a** Gene expression profiling was performed in KARPAS-422 cells treated with control shRNA or EZH2-specific shRNA for 10 days or with vehicle control or 500 nM GSK126 for 3 days. The heatmap represents unsupervised hierarchical clustering of normalized gene expression data for 1,778 probe sets that were significantly changed with either EZH2 knockdown or EZH2 inhibition. Green, lower expression. Red, higher expression. Differentially-regulated probe sets are included in Supplementary Table 6. **b** Venn diagram depicting the overlap of gene expression changes meeting criteria for significant up-regulation (FDR adjusted p-value < 0.1, > 2-fold change). Among the 393 probe sets that changed > 2-fold with GSK126 treatment but not with EZH2 knockdown, 185 were up-regulated ≥ 1.5-fold with shEZH2. **c** To determine the extent to which each class of genes identified in **b** was enriched for EZH2 target genes, H3K27me3 enrichment was evaluated using ChIP-Seq data from KARPAS-422 cells. Both commonly up-regulated and GSK126 only up-regulated gene sets were enriched above the "All" transcripts background; however, shEZH2 only up-regulated genes were not, suggesting that they represent off-target effects of the shRNA or secondary gene expression changes due to the longer treatment duration required for stable knockdown.
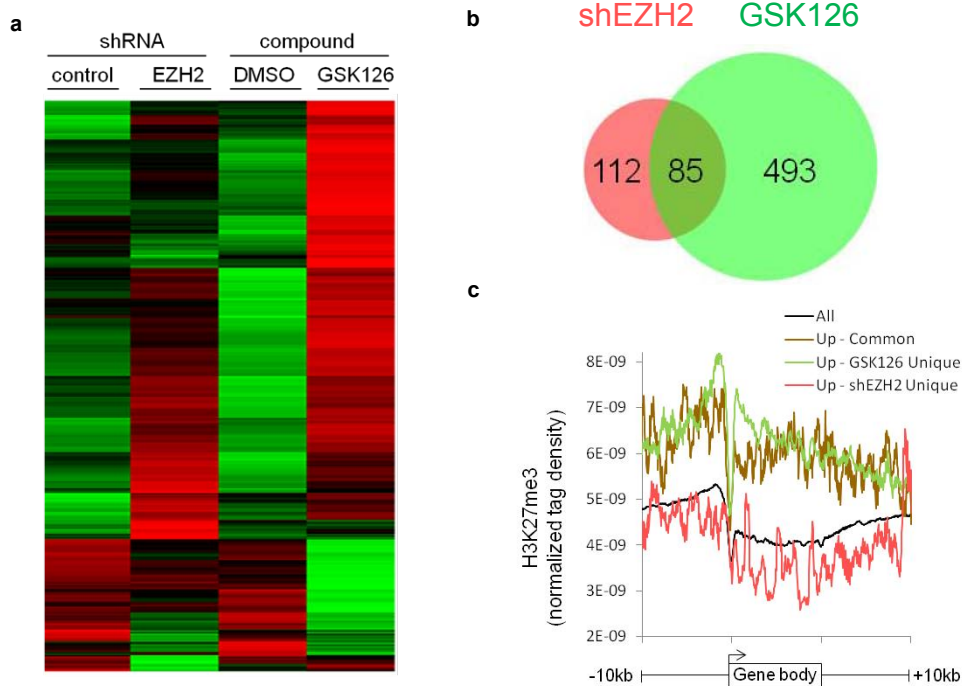
Supplementary Figure 10 | Comparison of gene expression changes elicited by EZH2 knockdown versus treatment with GSK126 in Pfeiffer. **a** Gene expression profiling was performed in Pfeiffer cells treated with control shRNA or EZH2-specific shRNA for 10 days or with vehicle control or 500 nM GSK126 for 3 days. The heatmap represents unsupervised hierarchical clustering of normalized gene expression data for probe sets that were significantly changed with either EZH2 knockdown or EZH2 inhibition. Green, lower expression. Red, higher expression. Differentially-regulated probe sets are included in Supplementary Table 6. **b** Venn diagram depicting the overlap of gene expression changes meeting criteria for significant up-regulation (FDR adjusted p-value < 0.1, > 2-fold change). Among the 493 probe sets that changed > 2-fold with GSK126 treatment but not with EZH2 knockdown, 165 were up-regulated ≥ 1.5-fold with shEZH2. **c** To determine the extent to which each class of genes identified in **b** was enriched for EZH2 target genes, H3K27me3 enrichment was evaluated using ChIP-Seq data from Pfeiffer cells. Both commonly up-regulated and "GSK126 unique" up-regulated gene sets were enriched above the "All" transcripts background; however, "shEZH2 Unique" up-regulated genes were not, suggesting that they represent off-target effects of the shRNA or secondary gene expression changes due to the longer treatment duration required for stable knockdown.
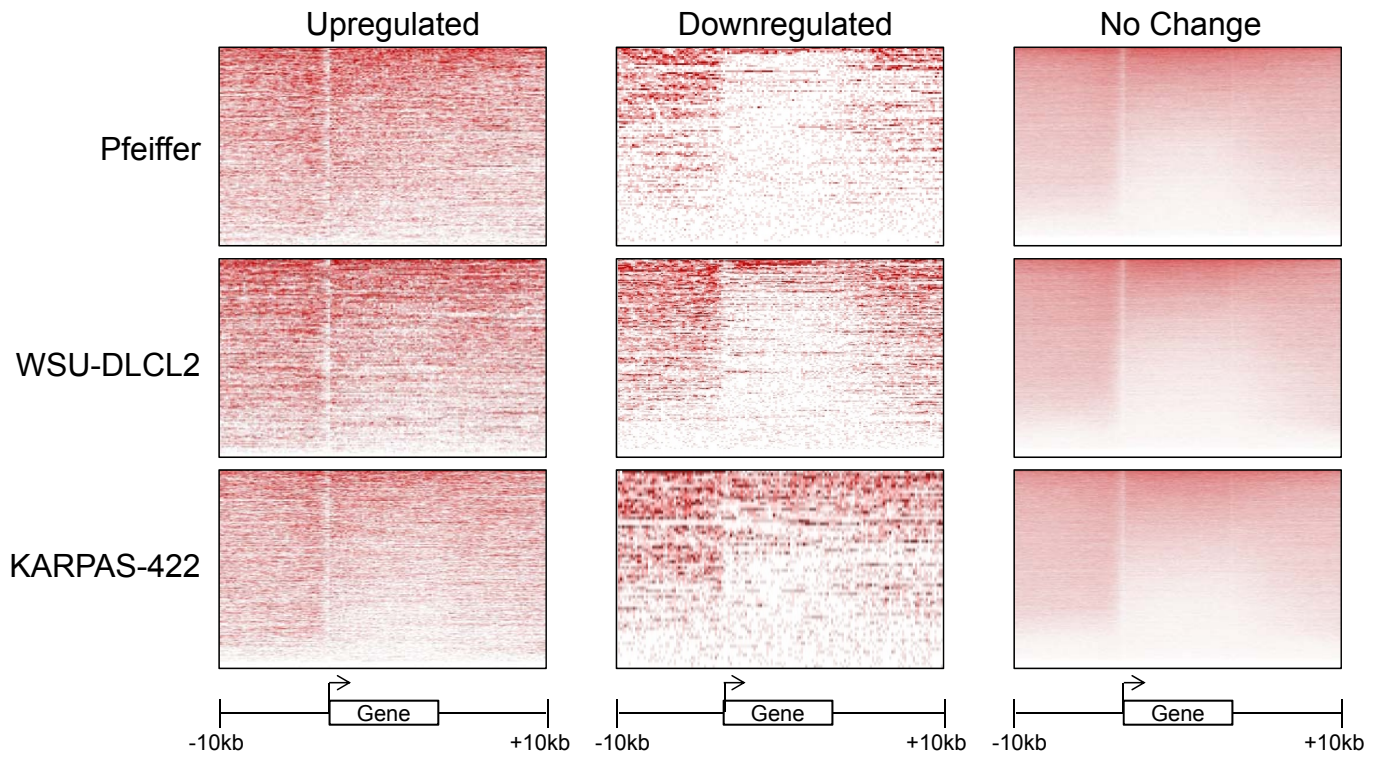
Supplementary Figure 11 | Genes up-regulated in response to GSK126 are enriched for H3K27me3. Probe sets that were significantly up-regulated, down-regulated, or unchanged identified in Pfeiffer, WSU-DLCL2, and KARPAS-422 cells following 72 hours with 500 nM GSK126 were mapped to individual genes and H3K27me3 enrichment determined for each gene and ±10kb from H3K27me3 ChIP-seq data. Relative H3K27me3 enrichment is represented as a white to red gradient with white representing no enrichment and red representing the highest enrichment. Each row represents a unique gene.

a

b
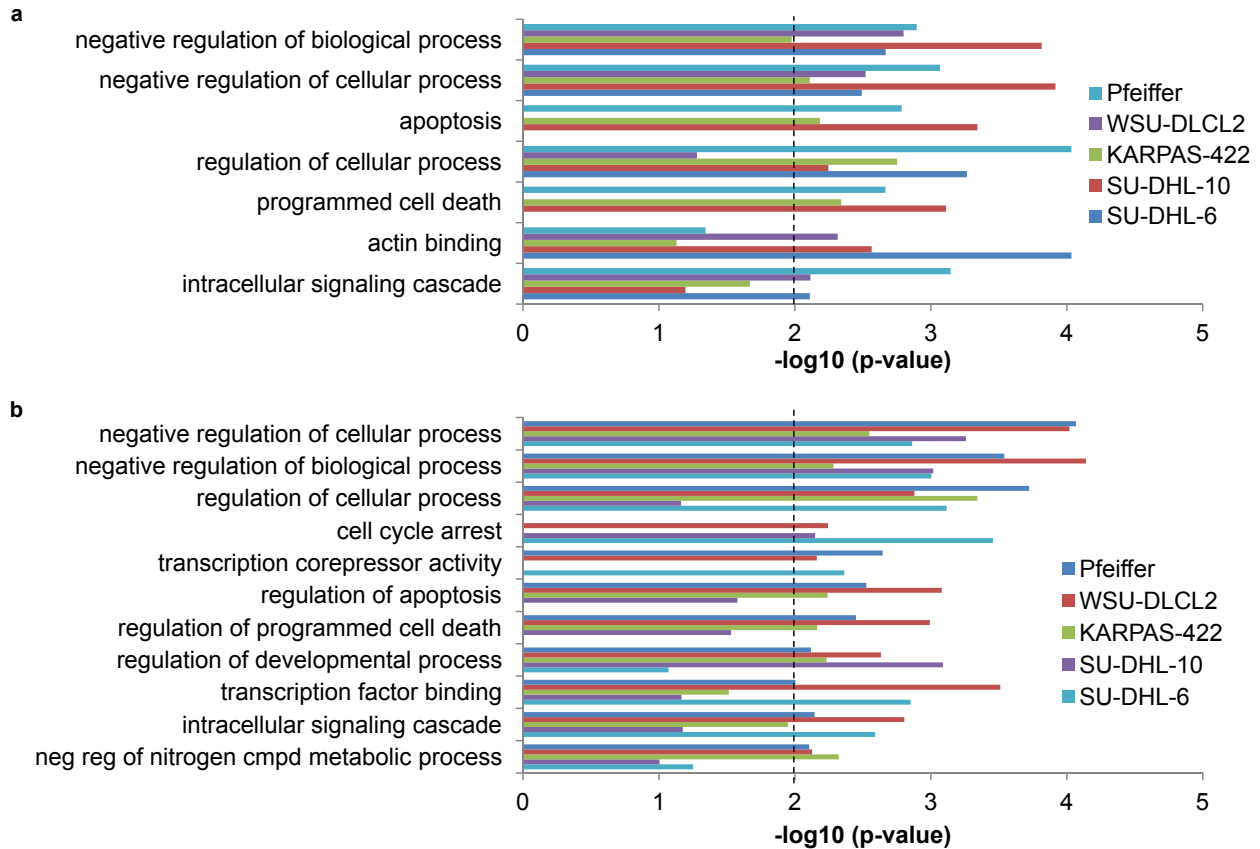
Supplementary Figure 12 | Gene ontology enrichment analysis. **a** GO enrichment analysis for probe sets significantly up-regulated with 500 nM GSK126 in Pfeiffer, WSU-DLCL2, KARPAS-422, SU-DHL-10, or SU-DHL-6. **b** GO enrichment analysis for probe sets either significantly up- or down-regulated with 500 nM GSK126 in Pfeiffer, WSU-DLCL2, KARPAS-422, SU-DHL-10, or SU-DHL-6. Over-represented biological process and molecular function terms were filtered for p-value < 0.01 (dashed lines), at least 5 genes per term, and those that were common across ≥ 3 cell lines.

a
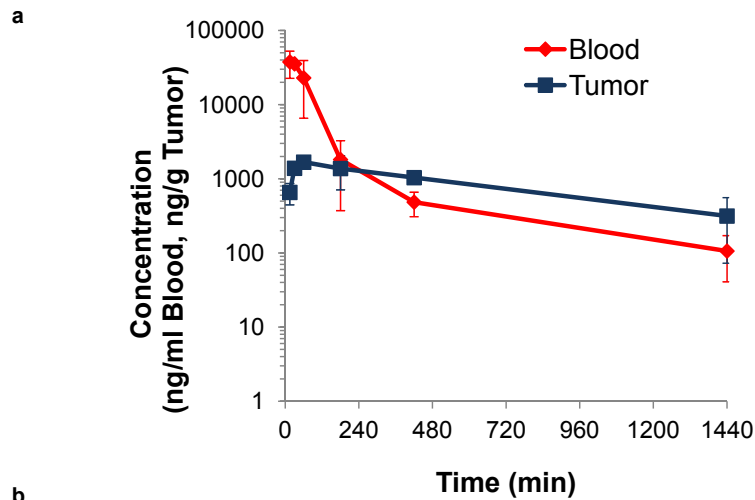
b

	AUC$_{0-1440}$ (ng*h/mL blood or ng*h/g tumor)	Ratio (tumor AUC/Blood AUC)	C$_{max}$ (ng/mL blood, ng/g tumor)	T$_{max}$ (min)
Blood	53189	N/A	37667 ± 15040	15
Tumor	19251	0.4	1678 ± 211	60

Supplementary Figure 13 | Pharmacokinetic analysis of GSK126. **a** Blood and tumor distribution following intraperitoneal administration of 50 mg per kg GSK126 to female beige SCID mice bearing Pfeiffer xenografts. Three mice were evaluated at each time point. **b** Area under the curve (AUC$_{0-1440}$), tumor/blood AUC ratio, maximum concentration achieved (C$_{max}$), and time of maximum concentration (T$_{max}$) for the data presented in **a**. N/A, not applicable.

a Pfeiffer
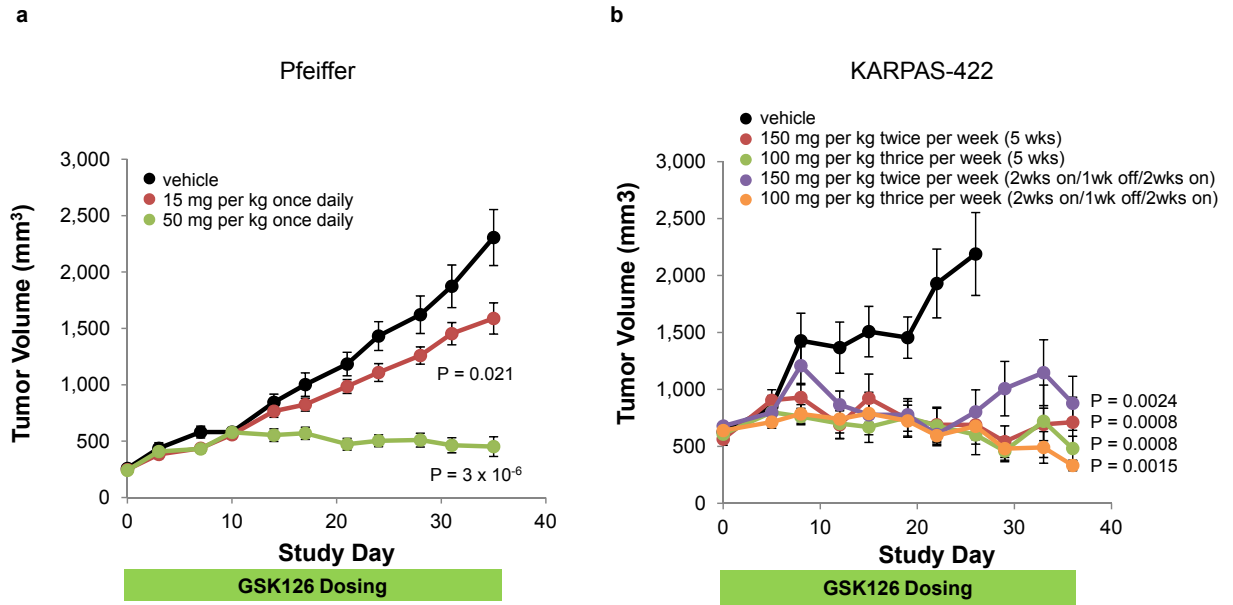
b KARPAS-422

Supplementary Figure 14 | GSK126 inhibits tumor growth *in vivo*. **a** Efficacy of GSK126 on the growth of subcutaneous Pfeiffer xenografts. **b** Efficacy of intermittent dosing of GSK126 on the growth of subcutaneous KARPAS-422 xenografts with or without a 1 week drug holiday. Values are the mean tumor volume ± standard error (n=10). P values were calculated using a nonparametric log-rank test comparing vehicle and each treatment group.
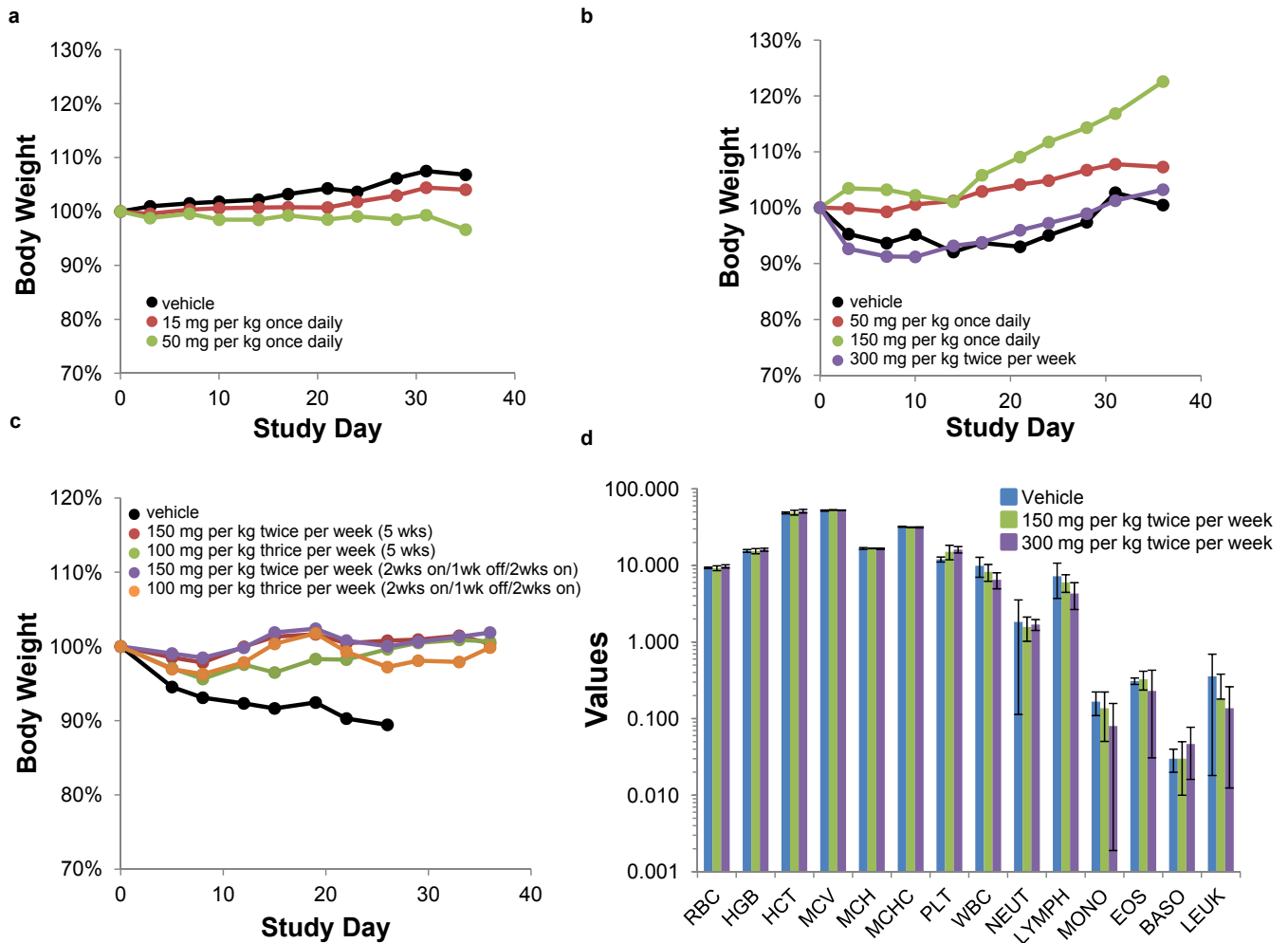
Supplementary Figure 15 | Effect of GSK126 on body weight and peripheral blood. **a-c** Average body weight measurements of mice bearing Pfeiffer (**a**) or KARPAS-422 (**b,c**) subcutaneous xenografts during treatment with vehicle or GSK126. Values are represented as a percentage of the average weight at the start of dosing. **d** Complete blood count analysis of CD-1 mice following twice weekly dosing over 18 days. RBC, red blood cells ($\times 10^6$ cells/μl); HGB, hemoglobin (g/dl); HCT, hematocrit (percent); MCV, mean corpuscle volume (fl); MCH, mean corpuscle hemoglobin (pg); MCHC, mean corpuscle hemoglobin concentration (g/dl); PLT, platelets ($\times 10^5$ platelets/μl); WBC, white blood cells ($\times 10^3$ cells/μl); NEUT, neutrophils ($\times 10^3$ cells/μl); LYMPH, lymphocytes ($\times 10^3$ cells/μl); MONO, monocytes ($\times 10^3$ cells/μl); EOS, eosinophils ($\times 10^3$ cells/μl); BASO, basophils ($\times 10^3$ cells/μl); LEUK, leukocytes ($\times 10^3$ cells/μl).

a

b

-vehicle   + 500 nM GSK126
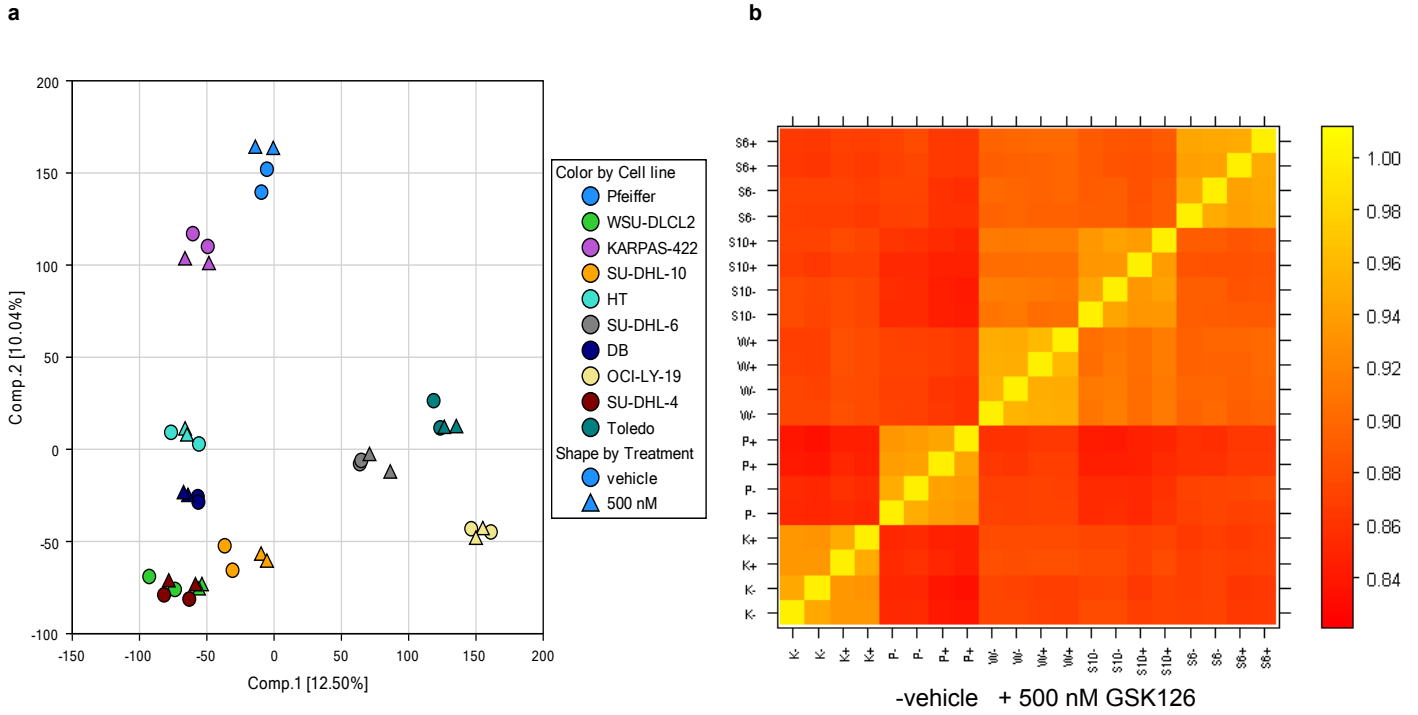
Supplementary Figure 16 | Principal component and correlation analysis of gene expression profiling data. **a** PCA plot of data from biological replicates of 10 DLBCL cell lines treated for 72 hours with vehicle or 500 nM GSK126. **b** Correlation of biological replicates of DLBCL cell lines with robust transcriptional changes. K, KARPAS-422; P, Pfeiffer; W, WSU-DLCL2; S10, SU-DHL-10; S6, SU-DHL-6.
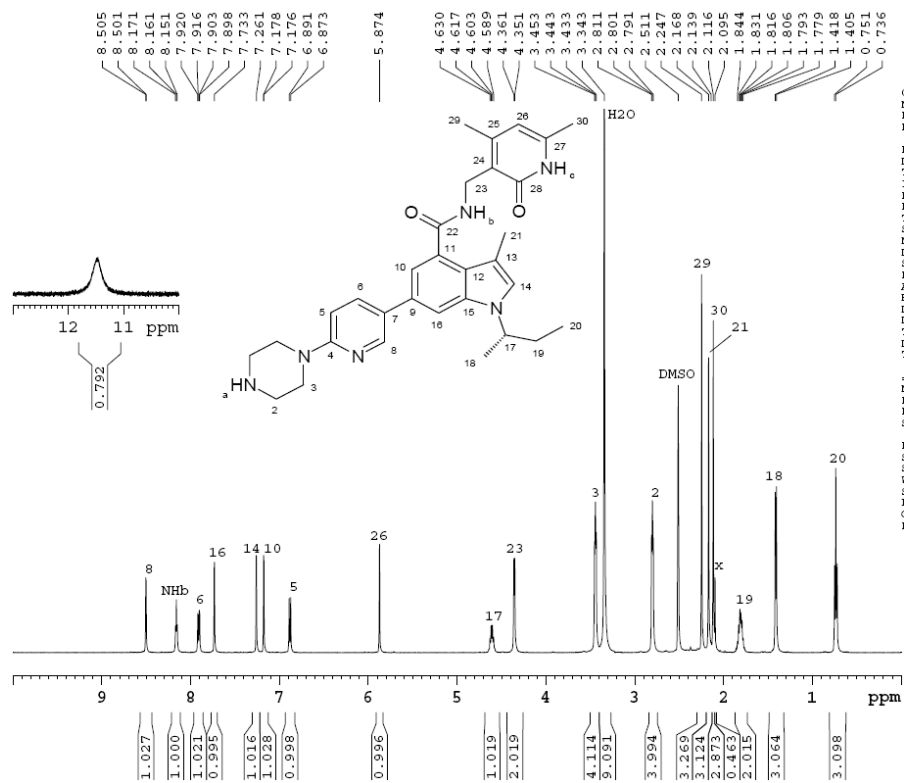
Supplementary Figure 17 | ^{1}H-NMR spectral image of GSK126. Spectra were recorded at 400 MHz.
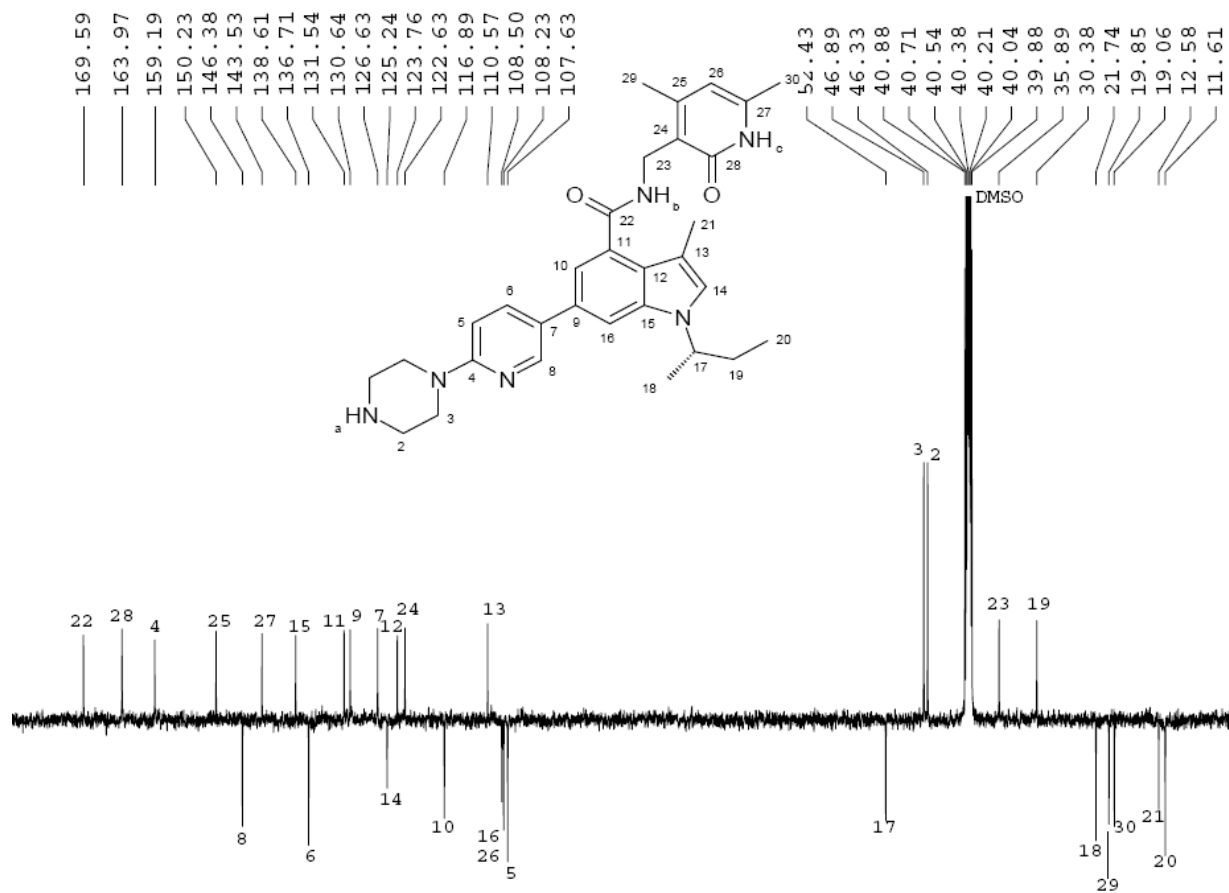
Supplementary Figure 18 | ^{13}C-NMR spectral image of GSK126. Spectra were recorded at 100 MHz.

Supplementary Methods

Chemistry

The following abbreviations are used throughout the experimental and have the following meaning:

aq	aqueous
BINAP	2,2' –bis(diphenylphosphino) –1,1'-binapthyl
ca.	circa
$CDCl_3$-*d*	chloroform-*d*
CD_3OD-*d*$_4$	methanol-*d*$_4$
Cs_2CO_3	cesium carbonate
$CHCl_3$	chloroform
ACN	acetonitrile
CH_3CN	acetonitrile
Celite®	registered trademark of Celite Corp. brand of diatomaceous earth
DBU	1,8-diazabicyclo[5.4.0]undeca-7-ene
DCE	dichloroethane
DCM	methylene chloride
DME	1,2 dimethoxyethane
DMF	N,N-dimethylformamide
DIEA	diisopropyl ethylamine
DMSO-*d*$_6$	dimethylsulfoxide-*d*$_6$
EtOAc	ethyl acetate
EDC	1-(3-dimethylaminopropyl)-3-ethylcarbodimmide hydrochloride
h	hour(s)
^{1}H NMR	proton nuclear magnetic resonance
HCl	hydrochloric acid
HOAT	1-hydroxy-7-azabenzotriazole
HPLC	high performance liquid chromatography
IPA	2-propanol
K_2CO_3	potassium carbonate
KOH	potassium hydroxide
LC/MS	liquid chromatography/mass spectroscopy
$MgSO_4$	magnesium sulfate
MeOH	methanol
min	minute(s)
MTBE	methyl tert-butyl ether
MS	mass spectrometry
NaOH	sodium hydroxide

Na$_2$SO$_4$	sodium sulfate
NH$_4$OH	ammonium hydroxide
NMM	4-methylmorpholine
NMP	N-Methyl-2-pyrrolidone
Pd/C	Palladium (10% by wt) on carbon
PdCl$_2$(dppf)-CH$_2$Cl$_2$	1,1'-Bis(diphenylphosphino)ferrocene-palladium(II)dichloride dichloromethane complex
Pd(Ph$_3$P)$_4$	tetrakis(triphenylphosphine)palladium(0)
RT	room temperature
SOCl$_2$	thionyl chloride
SPhos	2-Dicyclohexylphosphino-2',6'-dimethoxybiphenyl
TFA	trifluoroacetic acd
THF	tetrahydrofuran
TLC	thin layer chromatography

The following guidelines apply to all chemistry experimental procedures described herein. All reactions were conducted under a positive pressure of nitrogen using oven-dried glassware, unless otherwise indicated. Temperatures designated are external (i.e. bath temperatures), and are approximate. Air and moisture-sensitive liquids were transferred *via* syringe. Reagents were used as received, and sources for lesser known commercially available reagents are listed. Solvents utilized were those listed as "anhydrous" by vendors. Molarities listed for reagents in solutions are approximate, and were used without prior titration against a corresponding standard. All reactions were agitated by stir bar, unless otherwise indicated. Heating was conducted using heating baths containing silicon oil, unless otherwise indicated. Reactions conducted by microwave irradiation (0 – 400 W at 2.45 GHz) were done so using a Biotage Initiator^{TM} 2.0 instrument with Biotage microwave EXP vials (0.2 – 20 mL) and septa and caps. Irradiation levels utilized (i.e. high, normal, low) based on solvent and ionic charge were based on vendor specifications. Cooling to temperatures below -70 °C was conducted using dry ice/acetone or dry ice/2-propanol. Magnesium sulfate and sodium sulfate used as drying agents were of anhydrous grade, and were used interchangeably. Solvents described as being removed "*in vacuo*" or "under reduced pressure" were done so by rotary evaporation.

Preparative normal phase silica gel chromatography was carried out using either a Teledyne ISCO CombiFlash Companion instrument with RediSep or ISCO Gold silica gel cartridges (4 g-330 g), or an Analogix IF280 instrument with SF25 silica gel cartridges (4 g – 3-00g), or a Biotage SP1 instrument with HP silica gel cartridges (10g – 100 g). Purification by reverse phase HPLC was conducted using a YMC-pack column (ODS-A 75x30mm) as solid phase, unless otherwise noted. A mobile phase of 25mL/min A

(acetonitrile-0.1%TFA): B (water-0.1% TFA), 10-80% gradient A (10 min) was utilized with UV detection at 214 nM, unless otherwise noted.

A PE Sciex API 150 single quadrupole mass spectrometer (PE Sciex, Thornhill, Ontario, Canada) was operated using electrospray ionization in the positive ion detection mode. The nebulizing gas was generated from a zero air generator (Balston Inc., Haverhill, MA, USA) and delivered at 65 psi and the curtain gas was high purity nitrogen delivered from a Dewar liquid nitrogen vessel at 50 psi. The voltage applied to the electrospray needle was 4.8 kV. The orifice was set at 25 V and mass spectrometer was scanned at a rate of 0.5 scan/sec using a step mass of 0.2 amu and collecting profile data.

Method A LCMS. Samples were introduced into the mass spectrometer using a CTC PAL autosampler (LEAP Technologies, Carrboro, NC) equipped with a hamilton 10 uL syringe which performed the injection into a Valco 10-port injection valve. The HPLC pump was a Shimadzu LC-10ADvp (Shimadzu Scientific Instruments, Columbia, MD) operated at 0.3 mL/min and a linear gradient 4.5% A to 90% B in 3.2 min. with a 0.4 min. hold. The mobile phase was composed of 100% (H_2O 0.02% TFA) in vessel A and 100% (CH_3CN 0.018% TFA) in vessel B. The stationary phase is Aquasil (C18) and the column dimensions were 1 mm x 40 mm. Detection was by UV at 214 nm, evaporative light-scattering (ELSD) and MS.

Method B, LCMS. Alternatively, an Agilent 1100 analytical HPLC system with an LC/MS was used and operated at 1 mL/min and a linear gradient 5% A to 100% B in 2.2 min with a 0.4 min hold. The mobile phase was composed of 100% (H_2O 0.02% TFA) in vessel A and 100% (CH_3CN 0.018% TFA) in vessel B. The stationary phase was Zobax (C8) with a 3.5 um particle size and the column dimensions were 2.1 mm x 50 mm. Detection was by UV at 214 nm, evaporative light-scattering (ELSD) and MS.

Method C, LCMS. Alternatively, an MDSSCIEX API 2000 equipped with a capillary column of (50 × 4.6 mm, 5 μM) was used. HPLC was done on Agilent-1200 series UPLC system equipped with column Zorbax SB-C18 (50 x 4.6 mm, 1.8 μM) eluting with CH_3CN: ammonium acetate buffer. The reactions were performed in the microwave (CEM, Discover).

^{1}H-NMR spectra were recorded at 400 MHz using a Bruker AVANCE 400 MHz instrument or at 500 MHz using a Bruker DRX 500 MHz instrument, at 25 °C using a 5 mm 1H-13C/15N/D Z-GRAD TXI cryoprobe. ^{13}C-NMR spectra were recorded at 100 MHz using a Bruker AVANCE 400 MHz instrument or at 125.7 MHz using a Bruker DRX 500 MHz instrument. For ^{1}H-NMR spectra, multiplicities indicated are: s=singlet, d=doublet, t=triplet, q=quartet, quint= quintet, sxt= sextet, m=multiplet, dd = doublet of doublets, dt=doublet of triplets etc. and br indicates a broad signal. All spectra (**Supplementary Fig. 17**

and 18) were collected by means of standard Bruker programs, and with ACD Spect manager v. 10 used for reprocessing.

Analytical HPLC: Products were analyzed by Agilent 1100 Analytical Chromatography system, with 4.5 x 75 mm Zorbax XDB-C18 column (3.5 um) at 2 mL/min with a 4 min gradient from 5% CH_3CN (0.1% trifluoroacetic acid) to 95% CH_3CN (0.1% trifluoroacetic acid) in H_2O (0.1% trifluoroacetic acid) and a 1 min hold.

High Resolution Mass Spec was completed on a Waters (Milford, MA) qTOF Premiere Mass Spectrometer operating in W mode (resolving power ~15,000). Positive ion electrospray ionization is employed. Mass error (within 3mDa or 5ppm) and isotope fit considered to confirm formula. Melting points were taken from crystalline material using Thomas Hoover capillary melting point apparatus (Serial # 84T-096), and are uncorrected. Optical Rotations were performed using Jasco P-2000 Polarimeter **(**Serial #: A002361232**).** Samples were dissolved in methanol with a sample concentration of 10.00 mg/mL. Elemental (CHN) analysis was conducted at Intertek, (Whitehouse, New Jersey).

The compounds were named using ACD Name software [Advanced Chemistry Development, Inc., (ACD/Labs), Toronto, Canada. (http://www.acdlabs.com/products/name_lab/)].

Preparation of GSK126

Methyl 5-bromo-2-methyl-3-nitrobenzoate (2)

To a stirred solution of 2-methyl-3-nitro benzoic acid (300 g, 1647 mmol) in conc. H_2SO_4 (1.5 L) was added 1,3-dibromo-5,5 dimethyl -2,4-imadazolidinedione (258 g, 906 mmol) and the mixture was stirred at room temperature for 5 h. The reaction mixture was slowly added to ice water (4 L), and solid was

precipitated out. The solid was filtered off and washed with water (1.2 L), pet ether (1 L) and dried to afford the title compound **2** as a white solid (411 g, 96%), which was used without further purification. ^{1}H NMR (DMSO, 400 MHz) : δ 2.446 (s, 3H), 8.136 (s, 1H), 8.294 (s, 1H). LCMS (ES) m/z = 257.93 (M-H)[-]

Methyl 6-bromo-1H-indole-4-carboxylate (3)

To a stirred solution of **2** (140 g, 538.4 mmol) in DMF (550 ml) was added DMF-DMA (599 mL, 4846 mmol) at room temperature. The reaction mixture was stirred at 115 $^{\circ}$C for 18 h. The reaction mixture was then concentrated in vacuo. The residual contents (176 g, 536.5 mmol) were dissolved in acetic acid (696 mL) and added to a suspension of iron (329.2 g, 5902 mmol) in acetic acid (1.4 L) at 50 $^{\circ}$C. After completion of addition, the reaction mixture was stirred at 80-90 $^{\circ}$C for 4 h. The reaction mixture was then filtered through a Celite pad. The filtrate was poured onto ice water (1 L) and extracted with diethyl ether (3 x 700 ml). The combined organic layers were washed with sat NaHCO$_3$, brine, and dried over anhydrous Na$_2$SO$_4$, filtered, and evaporated under vacuum. The crude product was purified by silica gel chromatography (eluent: 10% ethyl acetate in pet ether) and afforded the title compound **3** as a solid (80 g, 59%). ^{1}H NMR (DMSO-d6, 400 MHz) δ: 3.980 (s, 3H), 7.168 (d, J = 3.2 Hz, 1H), 7.334 (d, J = 3.2 Hz, 1H), 7.734 (s, 1H), 8.017 (s, 1H), 8.384 (brs, 1H); LCMS (ES-) m/z = 251.9 (M-H).

Methyl 6-bromo-1-(sec-butyl)-1H-indole-4-carboxylate (4)
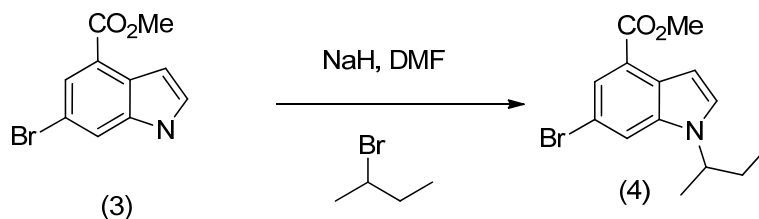
To a stirred suspension of sodium hydride (5.66 g, 141.7 mmol) in DMF (100 mL) was added a solution of **3** (30 g, 118.1 mmol) in DMF (50 mL) at 0 $^{\circ}$C and stirred for 20 min. Then 2-bromobutane (29.1 g, 212.5 mmol) was added at 0 $^{\circ}$C and the reaction mixture was stirred at room temperature for 16 h. The reaction mixture was diluted with cold water and extracted with ethyl acetate (4 x 150 mL). The combined organic layer was washed with cold water (150 mL), brine (100 mL) and dried over anhydrous Na$_2$SO$_4$ and concentrated under reduced pressure to afford crude product, which was purified by column

chromatography over silica gel (60-120 mesh) using 5% EtOAc: Pet ether as eluent to afford the title compound **4**, (14 g, 40.1%) as pale yellow solid. ^{1}H NMR (CDCl$_3$,400 MHz) δ 0.843-0.870 (m,3H), 1.512 (d, J = 6.4 Hz,3H), 1.844-1.926 (m, 2H), 3.976 (s, 3H), 4.333 - 4.385 (m, 1H), 7.132 (d, J = 3.2 Hz,1H), 7.302 (d, J = 3.6 Hz,1H), 7.707 (s, 1H), 7.984 (d, J = 1.6 Hz, 1H).

Methyl 6-bromo-1-(sec-butyl)-3-formyl-1H-indole-4-carboxylate (5)

(4)   POCl$_3$, DMF   (5)
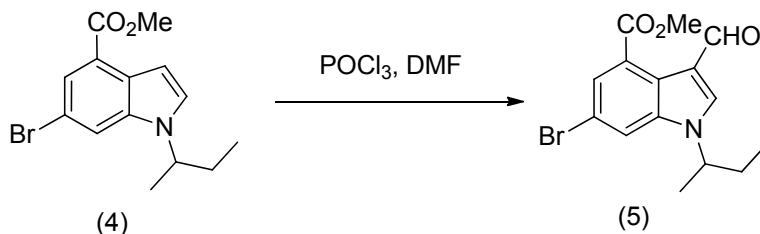
POCl$_3$ (8.3 g, 54.3 mmol) was added at 0°C to anhydrous DMF (230 mL) in a round bottom flask and stirred for 30 min. Then a solution of **4** (14 g, 45.3 mmol) in DMF (60 mL) was added to the reaction mixture at 0 °C and stirred at room temperature for 2.5 h. The reaction mixture was diluted with cold water, adjusted pH~8 using with 2N NaOH solution and extracted with ethyl acetate (4 x 200 mL). The combined organic layer was washed with cold water (2 x 100 mL), brine (100 mL), dried over anhydrous Na$_2$SO$_4$ and concentrated under reduced pressure to afford **5** (15.2 g, 99%) as pale yellow solid. This was used as such in the next step without purification. ^{1}H NMR (CDCl3 ,400 MHz) δ (0.831-0.859 (m, 3H), 1.515-1.574 (d, J = 6.8 Hz,3H), 1.729-1.972 (m, 2H) 3.997 (s, 3H), 4.394-4.445 (m, 1H), 7.756 (d, J = 1.2 Hz, 1H), 7.958 (d, J = 2 Hz, 1H), 8.079 (s, 1H), 10.452 (s, 1H).

Methyl 6-bromo-1-(sec-butyl)-3-methyl-1H-indole-4-carboxylate (6)

(5)   1)p-TsOH,p-tolsulfonyl hydrazide sulfolane, DMF 2) NaBH$_3$CN   (6)
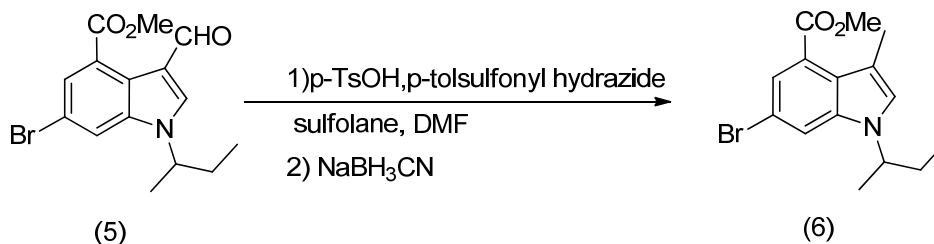
To a stirred solution of **5** (15 g, 44.6 mmol) in DMF (115 mL) was added *p*-toluenesulfonic acid monohydrate (1.1 g, 5.8 mmol), *p*-toluenesulfonyl hydrazide (10.8 g, 58 mmol) followed by sulfolane (115 mL) at RT and the reaction mixture was stirred at 100°C for 1 h. The reaction mixture was cooled to room temperature, treated with sodium cyanoborohydride (11.9 g, 178.5 mmol) portion wise over a period of 5 min and stirred at 100°C for 2 h. The reaction mixture was cooled to room temperature and stirred at the same temperature for 16 h. The reaction mixture was diluted with water and extracted with 30% EtOAc: Pet ether. The organic layer was washed with cold water (100 mL), brine (100 mL) and dried over anhydrous Na$_2$SO$_4$ and concentrated under reduced pressure to afford the crude product, which was

purified by column chromatography over silica gel (100-200 mesh) using 5% EtOAc: Pet ether as eluent to afford title compound **6** (7.88 g, 54.6%) as pale yellow gum. ^{1}H NMR (CDCl$_3$,400 MHz): δ 0.804-0.841(t, J=7.4 Hz, 3H),1.454-1.470 (d, J = 6.4 Hz, 3H), 1.865-1.884 (m, 2H), 2.363 (s, 3H), 3.950 (s, 3H), 4.265 - 4.316 (m, 1H), 7.038 (s, 1H), 7.609 (d, J = 1.2 Hz, 1H), 7.671 (d, J = 2 Hz, 1H). MS (ES+): 324.19 [M+H] ion present.

6-bromo-1-(sec-butyl)-3-methyl-1H-indole-4-carboxylic acid (7)

(6)   (7)
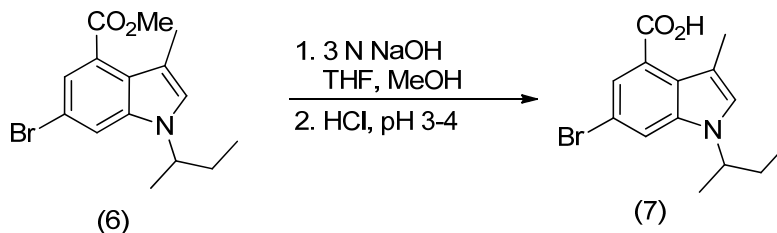
Compound **6** (3.24 g, 9.99 mmol) was dissolved in methanol (30 mL) and tetrahydrofuran (THF) (7 mL). The contents were stirred for 5 min., and then aq. 3N NaOH (19.99 mL, 60.0 mmol) was added via addition funnel over 3 min. The contents rapidly became a yellow suspension and were stirred at room temperature for 65 h. The volatiles were removed in vacuo and the residue dissolved in water (60 mL). The contents were washed with ether (1 x 50 mL). The aq layer was cooled in an ice bath and adjusted to pH 3-4 with 1M HCl, from which an oily residue precipitated. The contents were extracted with EtOAc (2 x 60 mL). The combined organic layers were dried over magnesium sulfate, filtered through celite, and concentrated *in vacuo*. The residue obtained was treated with TBME, concentrated i*n vacuo*, and then dried under hi vacuum to afford **7** as a yellow foam as 3.08 g (93%). ^{1}H NMR (400 MHz, DMSO-*d*6) δ ppm 0.70 (t,*J*=7.33 Hz, 3H), 1.39 (d, *J*=6.82 Hz, 3H), 1.71 - 1.86 (m, 2H), 2.30 (s, 3H), 4.48 - 4.62 (m, 1H), 7.40- 7.49 (m, 2H), 7.96 (d, *J*=1.77 Hz, 1H), 12.99 (s, 1H); LCMS = 310.0/312.0 (MH+).

(S)-6-bromo-1-(sec-butyl)-N-((4,6-dimethyl-2-oxo-1,2-dihydropyridin-3-yl)methyl)-3-methyl-1H-indole-4-carboxamide (8)

(7)   (8)
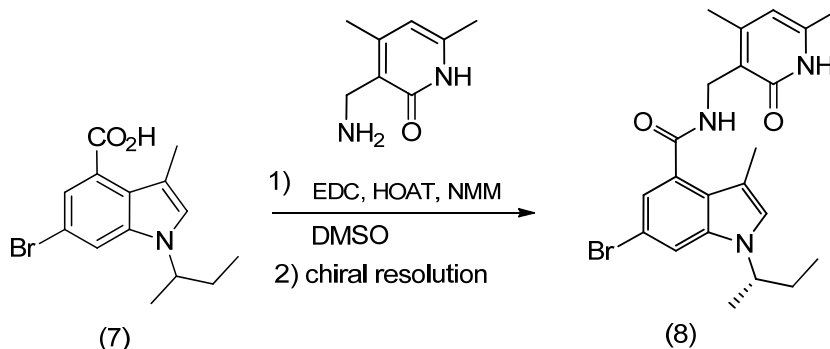
Added sequentially to a reaction flask were **7** (1.33 g, 4.29 mmol), 3-(aminomethyl)-4,6-dimethyl-2(1H)-pyridinone (1.213 g, 6.43 mmol), 1-hydroxy-7-azabenzotriazole (0.875 g, 6.43 mmol), EDC (1.233 g, 6.43

mmol), followed by DMSO (30 mL, via syringe) and then N methylmorpholine (1.886 mL, 17.15 mmol, via syringe). The contents were sealed and stirred at room temperature and the solids gradually dissolved. The contents were stirred at room temperature for 32 h, and then slowly diluted into 220 mL of ice-water with stirring. The contents were stirred for 10 min, and then allowed to stand for an additional 10 min. The contents were filtered and the filtered solid was washed with additional water (50 mL). The solid was then air dried for 10 min, and then in a vacuum oven at 50 °C for 23 h total. The product was collected as 1.75 g (87%). ^{1}H NMR (400 MHz, DMSO-d_6) δ ppm 0.69 (t, J=7.33 Hz, 3H), 1.36 (d, J=6.57 Hz, 3H), 1.77 (dq, J=10.29, 7.09 Hz, 2H), 2.12 (d, J=9.09 Hz, 6H), 2.21 (s, 3H), 4.30 (d, J=5.05 Hz, 2H), 4.43 - 4.56 (m, 1H), 5.86 (s, 1H), 6.99 (d, J=1.52 Hz, 1H), 7.30 (s, 1H), 7.77 (d, J=1.77 Hz, 1H), 8.25 (t, J=4.93 Hz, 1H), 11.49 (br. s.,1H); LCMS = 444.1 (MH+).   6-Bromo-1-(sec-butyl)-N-((4,6-dimethyl-2-oxo-1,2-dihydropyridin-3-yl)methyl)-3-methyl-1H-indole-4-carboxamide (racemic mixture, 1.9 g) was resolved by chiral HPLC (column : Chiralpak AD-H, 5 microns, 50 mm x 250 mm, UV detection :240 nM, flow rate: 100 mL/min, T = 20 deg C, eluent: 60:40:0.1 n-heptane:ethanol:isopropylamine (isocratic)). For each run, 100 mg of the racemic compound was dissolved in 30 volumes (3.0 mL) of warm ethanol with a few drops of isopropylamine added. A total of 19 runs were performed. Baseline resolution was observed for each run. The isomer that eluted at 8.3-10.1 min was collected (following concentration) as a white solid, which was dried at 50 °C (< 5 mm Hg) to afford 901 mg, and was determined to be the S isomer compound **8**.* (chiral HPLC: >99.5% ee (no R isomer detected). The isomer that eluted at 10.8-13.0 min was collected as a white solid, which was dried at 50 °C (< 5 mm Hg) to afford 865 mg, and was determined to be the R isomer.* ^{1}H NMR and LCMS were consistent with the parent racemate.   * The absolute configuration was determined by an independent synthesis of each enantiomer from the corresponding commercially available homochiral alcohols via Mitsunobu reaction.   The sterochemical assignments were also consistent by vibrational circular dichroism (VCD) analysis.

(S)-1-(sec-butyl)-N-((4,6-dimethyl-2-oxo-1,2-dihydropyridin-3-yl)methyl)-3-methyl-6-(6-(piperazin-1-yl)pyridin-3-yl)-1H-indole-4-carboxamide **(GSK126)**
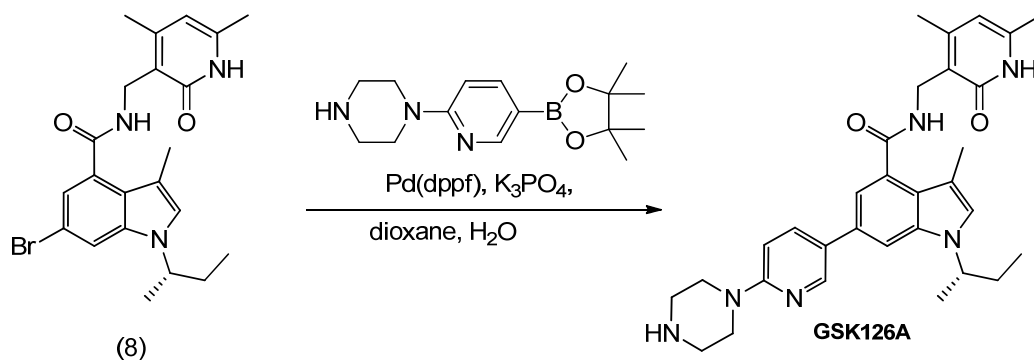
To a 30 mL microwave vial were added **8** (100 mg, 0.225 mmol), 1-(5-(4,4,5,5-tetramethyl-1,3,2-dioxaborolan-2-yl)pyridin-2-yl)piperazine (85 mg,0.293 mmol), 1,2-Dimethoxyethane (DME) (3 mL), water

(1.000 mL) and sodium carbonate (0.338 mL, 0.675 mmol), and the mixture was degassed for 5 min by bubbling nitrogen. $PdCl_2(dppf)$-CH_2Cl_2 adduct (14.70 mg, 0.018 mmol) was added and the tube was sealed. The mixture was irradiated (microwave) at 140 °C for 10 min. The mixture was concentrated and the residue was taken up into MeOH and filtered. The filtrate was purified using reverse phase HPLC (eluent: 25%ACN/H2O, 0.1% NH4OH to 60% ACN/H_2O, 0.1% NH_4OH) to give 91 mg of **GSK126** as off-white solid. m.p. = 260-261 °C; TLC (CH_2Cl_2:MeOH with 1% NH4OH added, 90:10 v/v): R_F = 0.16; $[\alpha]^D_{20}$ (deg cm^3 g^{-1} dm^{-1}) = −13.3 (c = 0.1 g cm^{-3} in CH_3OH); ^1H NMR (500 MHz, DMSO-d_6) δ ppm 8.50 (d, J=2.53 Hz, 1H), 8.16 (t, J=5.05 Hz, 1H), 7.91 (dd, J=8.84, 2.53 Hz, 1H), 7.73 (d, J=1.26 Hz, 1H), 7.26 (s, 1H), 7.17 (d, J=1.52 Hz, 1H), 6.88 (d, J=8.84 Hz, 1H), 5.87 (s, 1H), 4.56 - 4.68 (m, 1H), 4.35 (d, J=5.31 Hz, 2H), 3.41 - 3.49 (m, 4H), 2.77 - 2.85 (m, 4H), 2.22 - 2.27 (m,3H), 2.16 (s, 3H), 2.11 (s, 3H), 1.75 - 1.87 (m, 2H), 1.37 - 1.44 (m, 3H), 0.70 - 0.78 (m, 3H); ^{13}C NMR (125 MHz, DMSO-d_6) δ 169.6 (CO), 164.0 (CO), 159.2 (C), 150.2 (C), 146.4 (CH), 143.5 (C), 138.6 (C), 136.7 (CH), 131.5 (C), 130.6 (C), 126.6 (C), 125.2 (CH), 123.8 (C), 122.6 (C), 116.9 (CH), 110.6 (C), 108.5 (CH), 108.2 (CH), 107.6 (CH), 52.4 (CH), 46.9 (2 CH_2), 46.3 (2 CH_2), 35.9 (CH_2), 30.4 (CH_2), 21.7 (CH_3), 19.9 (CH_3), 19.1 (CH_3), 12.6 (CH_3), 11.6 (CH_3); HRMS (m/z): $[MH]^+$ calcd for $C_{31}H_{39}N_6O_2$, 527.3134; found, 527.3134; CHN analysis (% calcd, % found for $C_{31}H_{38}N_6O_2$ 0.1 mol H_2O and 0.09 mol acetone): C (70.39, 70.44), H (7.27, 7.50), N (15.74, 15.80).

3-(Aminomethyl)-4,6-dimethyl-2(1*H*)-pyridinone hydrochloride (10)
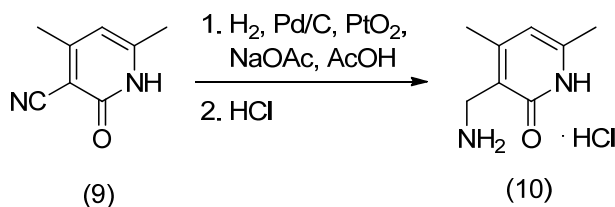
Palladium on carbon (10%) (3.24 g) was charged into a 2L dry Parr bottle and a small amount of acetic acid was added. Next added 4,6-dimethyl-2-oxo-1,2-dihydro- pyridine-3- carbonitrile (30 g , 202.7 mmol), sodium acetate (30.75 g, 375.0 mmol), platinum oxide (0.218 g), and acetic acid (1 L).. The bottle was capped, placed on Parr apparatus, and shaken under an atmosphere of H_2 (100 psi) for 2 days. The reaction mixture was filtered. The solvent was removed to give a residue, which was treated with 150 mL of conc. HCl, and the formed solids were filtered. The yellow filtrate was concentrated . To the crude compound was added 30 mL of conc. HCl and 150 mL EtOH, the contents cooled to 0 °C, and stirred at 0 °C for 2h. The formed solids were filtered, washed with cold EtOH, ether, and dried. The product was collected as 36 g. This batch was combined with other batches prepared on smaller scales and triturated with ether to give 51 g of pure compound **10**. ^1H NMR (400 MHz, DMSO-d_6) δ ppm 11.85 (br s,1 H) 8.13 (br s, 3 H) 5.93 - 6.01 (m, 1 H) 3.72 - 3.80 (m, 2 H) 2.22 (s, 3 H) 2.16 (s, 3 H).

Selectivity analysis of GSK126 in a panel of methyltransferases (HMTs). GSK126 was profiled at Reaction Biology Corp. (Malvern, PA) to assess inhibition in their panel of histone methyltransferase assays (**Supplementary Table 1**). Methyltransferase activity was assessed using HotSpot technology, a miniaturized radioisotope-based filter binding assay. GSK126 was dissolved in dimethyl sulfoxide (DMSO) and tested at concentrations up to 100 µM with a final DMSO concentration of 2%. Buffer containing the methyltransferase and its preferred substrate (histone H4 for PRMT1, core histones for DOT1L, MLL1, MLL2, MLL3, and MLL4, or histone H3 for the remaining enzymes, lambda DNA for DNMT1 and DNMT3a/b) was pre-incubated with GSK126 for 10 minutes. Reactions were initiated by the addition of 1 µM S-adenosyl-L-[methyl-^{3}H]methionine (SAM), allowed to incubate for 60 min at 30 $^{\circ}$C followed by transfer to P81 filter-paper, and washed with PBS before detection.

Selectivity Analysis of GSK126 in a panel of histone acetyltransferases (HDACs). GSK was profiled at Reaction Biology Corp. to assess inhibition in their panel of histone deacetylase assays (**Supplementary Table 2**). Deacetylase activity was assessed using fluorogenic substrates. GSK126 was dissolved in dimethyl sulfoxide (DMSO) and tested at concentrations up to 100 µM with a final DMSO concentration of 2%. GSK126 was added to reaction plates containing the HDAC of interest in assay buffer. Reactions were initiated by addition of 50 µM of the fluorogenic substrate (an acetylated peptide substrate based on residues 379-382 of p53 (Arg-His-Lys-Lys(Ac)), incubated for 2 hr at 30 $^{\circ}$C before being developed.

Selectivity analysis of GSK126 in a panel of GPCRs and ion channels. Adenosine 2a, Adrenergic α1b, Serotonin 3 and α1 nicotinic ACHr activity were assessed in cultured whole cells loaded with calcium-sensitive dyes (**Supplementary Table 3**). Fluorescent output was monitored in real-time using a fluorometric imaging plate reader (FLIPR). Dopamine D2, µ Opioid and Serotonin 1B activity was assessed in a ^{35}S-GTPγS binding scintillation proximity assay using membranes prepared from cells expressing G$_i$-coupled 7TM receptors. Membranes were pre-coupled with GDP and beads, ^{35}S-labelled GTPγS was added to the mixture immediately before dispensing into plates containing test compounds (agonist format). After incubation, luminescence was determined in a Viewlux plate reader (Perkin Elmer). For antagonist assays, a standard agonist was added to the assay mix at the same time as [^{35}S]-GTPγS, and ablation of GTPγS-binding was assessed.

Selectivity analysis of Norepinephrine transporter (NET) [^{3}H]-nisoxetine binding to Bacmam membranes expressing human NET was measured using LEADSeeker beads (Perkin Elmer) (**Supplementary Table 3**).

Selectivity analysis of GSK126 in a panel of kinases. GSK was profiled at Reaction Biology Corp. to asses inhibition in their panel of kinases (**Supplementary Table 4**). Kinases activity was assessed using HotSpot technology, a miniaturized radioisotope-based filter binding assay. GSK126 was dissolved in dimethyl sulfoxide (DMSO) and tested at a single concentration of 10 µM with a final DMSO concentration of 2%. GSK126 was added to reaction plates containing the kinase of interest in assay buffer containing a suitable substrate for the given kinase (generally, either a polypeptide containing 9-40 amino acids, or a full length generic protein such as maltose binding protein (MBP), casein, or Histone H1). Reactions were initiated with 10 µCi/µL ^{33}P-ATP (total ATP concentration at K$_m$) incubated for 2 hr at RT. Completed

reactions were spotted on P81 ion exchange paper and washed with 0.75% phosphoric acid before detection.

shRNA-mediated EZH2 knockdown. Pfeiffer and KARPAS-422 cells plated in RPMI-1640 supplemented with 10% fetal bovine serum and 8 µg/ml polybrene were infected with lentiviral transduction particles (Sigma) containing shRNA specific for a non-mammalian control sequence or human EZH2. Sequences for the shRNA were as follows: shControl – CCGGCAACAAGATGAAGAGCACCAACTCGAGTTGGTGCTCTTCATCTTGTTGTTTTT and shEZH2 – CCGGTATGATGGTTAACGGTGATCACTCGAGTGATCACCGTTAACCATCATATTTTTG. Two days after the addition of virus, cells were transferred to RPMI-1640 media supplemented with 10% fetal bovine serum and 1 µg/ml puromycin to select for infected cells. After 2 days of puromycin selection, cells were plated into 96 well plates for analysis of cell proliferation and Caspase 3/7 activity using CellTiter-Glo (Promega) and Caspase-Glo 3/7 (Promega), respectively. For 6 days, plates were read daily using an EnVision multi-label plate reader (PerkinElmer) after a 30 minute incubation with CellTiter-Glo or Caspase-Glo 3/7 reagent. Triplicate wells were evaluated with each reagent at each time point and Caspase-3/7 activity was normalized to CellTiter-Glo signal. For gene expression profiling studies, KARPAS-422 cells were treated with control non-targeting shRNA or EZH2-specific shRNA for 10 days in duplicate, and cells were collected and processed as described below.

Supplementary Table 1: Inhibition of human methyltransferases by GSK126

Target Name	IC$_{50}$ (nM)[a]	K$_i$^{app} (nM)[b]
EZH2[cd]	9.9	0.57
EZH1[cd]	680	89
SET8[d]	13,000	ND[f]
MLL4[d]	25,000	ND
DNMT1[e]	29,490	ND
MLL1[d]	30,000	ND
SET7[d]	38,000	ND
SUV39H2[d]	86,000	ND
PRMT6[e]	88,000	ND
DOT1L[e]	>100,000	ND
G9A/EHMT2[d]	>100,000	ND
MMSET/NSD2[d]	>100,000	ND
PRMT1[e]	>100,000	ND
PRMT3[e]	>100,000	ND
PRMT4[e]	>100,000	ND
PRMT5[e]	>100,000	ND
SETMAR[d]	>100,000	ND
SMYD2[d]	>100,000	ND
SUV39H1[d]	>100,000	ND
MLL2[d]	>100,000	ND
MLL3[d]	>100,000	ND
DNMT 3a/3b[e]	>100,000	ND

[a] IC$_{50}$, the concentration of GSK126 resulting in 50% inhibition of enzyme activity.
[b] As the potency of GSK126 is at or near the tight binding limit of an assay run at [SAM] = K_m, IC$_{50}$ values were re-determined at a higher SAM concentration (7.5 μM) and apparent K_i values were calculated using the Cheng-Prusoff[1] relationship for a competitive inhibitor.
[c] Measured using 5-member complexes of EZH2 or EZH1 along with EED, SUZ12, AEBP2, RbAp48.
[d] SET domain containing methyltransferase
[e] Non-SET domain containing methyltransferase
[f] ND, not determined.

Supplementary Table 2: Inhibition of human histone deacetylases and demethylases by GSK126

Target Name	Protein Class	IC$_{50}$ (nM) [a]
HDAC1	HDAC	*
HDAC2	HDAC	*
HDAC3	HDAC	*
HDAC4	HDAC	>100,000
HDAC5	HDAC	*
HDAC6	HDAC	*
HDAC7	HDAC	*
HDAC8	HDAC	>100,000
HDAC9	HDAC	>100,000
HDAC10	HDAC	>100,000
HDAC11	HDAC	>100,000
JMJD2d	HDM	7,900
JMJD3	HDM	>50,000
LSD1	HDM	>100,000

[a] IC$_{50}$, the concentration of GSK126 resulting in 50% inhibition of enzyme activity.
* Indicates no inhibition or compound activity that could be fit to an IC$_{50}$ curve.

Supplementary Table 3: Activity of GSK126 against GPCRs, ion channels, and transporters

Protein Name	Protein Class	Assay Mode	GSK126 $EC_{50}/IC_{50}(\mu M)$ [a]
Serotonin 1B	GPCR	Agonist	>31.6
Serotonin 1B	GPCR	Antagonist	>31.6
Adenosine 2a	GPCR	Agonist	>31.6
Adrenergic α1b	GPCR	Antagonist	> 40
Dopamine D2	GPCR	Agonist	100
μ Opioid	GPCR	Agonist	>100
μ Opioid	GPCR	Antagonist	>100
Serotonin 3	Ion Channel	Blocker	4.0
Serotonin 3	Ion Channel	Opener	>50
α1 nicotinic AChR	Ion Channel	Opener	>50
Norepinephrine	Transporter	Antagonist	31.6

[a] EC_{50} and IC_{50}, the concentration of GSK126 resulting in 50% maximal effective or inhibitory activity, respectively.

Supplementary Table 4: Inhibition of kinases by GSK126

Kinase	% Enzyme Activity (relative to DMSO controls)[a] GSK126		IC_{50} (nM) Staurosporine[b]
	Data 1	Data 2	
ABL1	86	82	49
ABL2/ARG	89	87	16
ACK1	93	94	19
AKT1	94	88	3
AKT2	92	95	11
AKT3	96	92	3
ALK	93	90	2
ALK1/ACVRL1	96	100	3162
ALK2/ACVR1	99	86	3545
ALK4/ACVR1B	101	96	17630
ALK5/TGFBR1	100	100	>20000
ARAF	101	108	ND[c]
ARK5/NUAK1	102	102	<1.0
ASK1/MAP3K5	103	102	8
Aurora A	90	86	2
Aurora B	114	93	3
Aurora C	103	99	2
AXL	106	100	6
BLK	84	79	2
BMX/ETK	100	104	15
BRAF	97	94	ND
BRK	96	90	170

BRSK1	99	100	<1.0
BRSK2	104	102	<1.0
BTK	107	99	10
c-Kit	97	101	39
c-MER	101	96	13
c-MET	134	123	119
c-Src	84	83	2
CAMK1a	59	49	3
CAMK1b	89	87	8
CAMK1d	87	77	<1.0
CAMK1g	90	78	7
CAMK2a	99	108	<1.0
CAMK2b	96	95	<1.0
CAMK2d	99	101	<1.0
CAMK2g	99	100	<1.0
CAMK4	92	83	187
CAMKK1	101	91	14
CAMKK2	96	100	14
CDK1/cyclin A	94	91	5
CDK1/cyclin B	101	97	2
CDK2/cyclin A	98	96	<1.0
CDK2/cyclin E	96	96	2
CDK3/cyclin E	108	102	3
CDK4/cyclin D1	95	94	7
CDK4/cyclin D3	103	105	15
CDK5/p25	99	96	2

CDK5/p35	102	104	2
CDK6/cyclin D1	105	106	2
CDK6/cyclin D3	93	112	24
CDK7/cyclin H	103	100	162
CDK9/cyclin K	96	97	12
CDK9/cyclin T1	101	95	12
CHK1	78	80	<1.0
CHK2	102	40	3
CK1a1	102	92	7927
CK1d	104	96	ND
CK1epsilon	97	92	ND
CK1g1	106	113	5010
CK1g2	90	91	2001
CK1g3	98	98	1997
CK2a	113	106	ND
CK2a2	68	85	1368
CLK1	104	94	7
CLK2	91	88	2
CLK3	88	84	807
CLK4	94	97	24
COT1/MAP3K8	93	98	ND
CSK	92	87	12
CTK/MATK	99	92	1033
DAPK1	100	93	7
DAPK2	105	107	4
DCAMKL2	105	104	26

DDR2	103	102	23
DMPK	92	109	54
DRAK1/STK17A	96	97	15
DYRK1/DYRK1A	96	94	2
DYRK1B	86	95	<1.0
DYRK2	202	205	75
DYRK3	100	93	34
DYRK4	99	98	ND
EGFR	102	91	174
EPHA1	104	104	102
EPHA2	103	108	63
EPHA3	101	95	23
EPHA4	96	88	20
EPHA5	76	78	18
EPHA6	94	86	10
EPHA7	94	89	23
EPHA8	89	89	96
EPHB1	93	88	31
EPHB2	101	90	88
EPHB3	96	89	1067
EPHB4	96	94	158
ERBB2/HER2	103	97	150
ERBB4/HER4	102	85	277
ERK1	102	96	1651
ERK2/MAPK1	99	91	1951
FAK/PTK2	98	85	7

FER	84	87	1
FES/FPS	102	96	2
FGFR1	87	82	7
FGFR2	97	100	2
FGFR3	89	72	11
FGFR4	89	89	81
FGR	93	89	1
FLT1/VEGFR1	98	97	13
FLT3	92	83	<1.0
FLT4/VEGFR3	87	78	2
FMS	98	92	<1.0
FRK/PTK5	100	94	14
FYN	99	102	3
GCK/MAP4K2	93	90	<1.0
GRK2	113	103	452
GRK3	103	107	651
GRK4	99	97	102
GRK5	97	105	42
GRK6	105	103	39
GRK7	96	99	1
GSK3a	104	99	4
GSK3b	92	100	11
Haspin	102	94	6
HCK	105	97	1
HGK/MAP4K4	107	97	<1.0
HIPK1	99	99	ND

HIPK2	95	85	576
HIPK3	105	95	878
HIPK4	92	84	373
IGF1R	97	96	52
IKKa/CHUK	94	92	358
IKKb/IKBKB	102	102	604
IKKe/IKBKE	89	100	<1.0
IR	95	96	33
IRAK1	97	97	53
IRAK4	106	108	3
IRR/INSRR	91	85	14
ITK	93	86	12
JAK1	98	97	<1.0
JAK2	93	90	<1.0
JAK3	97	94	<1.0
JNK1	104	95	10840
JNK2	84	77	4150
JNK3	103	107	ND
KDR/VEGFR2	107	100	25
KHS/MAP4K5	106	98	<1.0
LCK	101	97	1
LIMK1	102	97	2
LKB1	105	108	30
LOK/STK10	91	89	7
LRRK2	96	102	5
LYN	98	109	2

LYN B	91	93	2
MAPKAPK2	99	99	174
MAPKAPK3	108	93	2217
MAPKAPK5/PRAK	80	92	651
MARK1	100	91	<1.0
MARK2/PAR-1Ba	94	91	<1.0
MARK3	111	109	<1.0
MARK4	82	84	<1.0
MEK1	106	99	7
MEK2	103	100	24
MEKK2	104	97	9
MEKK3	107	107	5
MELK	81	78	<1.0
MINK/MINK1	111	100	<1.0
MKK6	95	94	53
MLCK/MYLK	97	95	46
MLCK2/MYLK2	99	94	11
MLK1/MAP3K9	94	91	<1.0
MLK2/MAP3K10	104	102	2
MLK3/MAP3K11	96	94	1
MNK1	96	98	35
MNK2	104	92	12
MRCKa/CDC42BPA	103	98	4
MRCKb/CDC42BPB	102	100	4
MSK1/RPS6KA5	107	108	<1.0
MSK2/RPS6KA4	90	91	<1.0

MSSK1/STK23	97	99	2061
MST1/STK4	98	96	<1.0
MST2/STK3	89	91	<1.0
MST3/STK24	81	83	2
MST4	102	94	3
MUSK	105	103	73
MYO3b	94	90	6
NEK1	99	94	8
NEK11	112	102	199
NEK2	102	104	909
NEK3	107	107	>20000
NEK4	99	92	126
NEK6	97	94	ND
NEK7	100	99	ND
NEK9	106	97	106
NIK/MAP3K14	104	94	698
NLK	96	94	55
OSR1/OXSR1	96	89	78
P38a/MAPK14	103	97	ND
P38b/MAPK11	103	102	ND
P38d/MAPK13	100	90	168
P38g	102	93	219
p70S6K/RPS6KB1	100	94	<1.0
p70S6Kb/RPS6KB2	96	88	2
PAK1	104	108	<1.0
PAK2	97	98	<1.0

PAK3	95	92	<1.0
PAK4	98	97	6
PAK5	97	106	2
PAK6	100	103	54
PASK	88	93	11
PBK/TOPK	97	91	105
PDGFRa	104	95	<1.0
PDGFRb	106	97	2
PDK1/PDPK1	102	99	39
PHKg1	101	95	1
PHKg2	97	90	<1.0
PIM1	101	103	3
PIM2	101	97	30
PIM3	102	85	<1.0
PKA	109	94	<1.0
PKAcg	100	100	5
PKCa	103	110	<1.0
PKCb1	101	102	3
PKCb2	94	94	<1.0
PKCd	108	97	<1.0
PKCepsilon	100	99	<1.0
PKCeta	105	101	<1.0
PKCg	97	86	1
PKCiota	99	100	10
PKCmu/PRKD1	103	98	<1.0
PKCnu/PRKD3	110	95	<1.0

PKCtheta	101	98	<1.0
PKCzeta	101	98	52
PKD2/PRKD2	98	98	<1.0
PKG1a	96	94	1
PKG1b	91	90	1
PKG2/PRKG2	99	95	3
PKN1/PRK1	86	92	<1.0
PKN2/PRK2	91	88	1
PLK1	102	95	189
PLK2	94	93	3775
PLK3	114	98	225
PRKX	80	81	<1.0
PYK2	108	113	5
RAF1	101	93	ND
RET	100	97	<1.0
RIPK2	96	95	237
RIPK5	101	94	27
ROCK1	94	98	<1.0
ROCK2	104	93	<1.0
RON/MST1R	92	102	315
ROS/ROS1	120	101	<1.0
RSK1	84	68	<1.0
RSK2	95	86	<1.0
RSK3	95	89	<1.0
RSK4	104	80	<1.0
SGK1	98	100	9

SGK2	107	103	15
SGK3/SGKL	104	106	131
SIK2	111	105	<1.0
SLK/STK2	112	104	9
SNARK/NUAK2	107	99	19
SRMS	102	85	12610
SRPK1	106	110	45
SRPK2	100	97	228
STK16	102	101	96
STK22D/TSSK1	97	108	<1.0
STK25/YSK1	92	94	1
STK33	94	95	23
STK38/NDR1	100	94	11
STK39/STLK3	98	93	22
SYK	93	85	<1.0
TAK1	104	107	43
TAOK1	93	90	<1.0
TAOK2/TAO1	105	101	4
TAOK3/JIK	104	98	<1.0
TBK1	105	105	<1.0
TEC	89	74	643
TGFBR2	96	104	15490
TIE2/TEK	97	94	85
TLK2	97	105	2
TRKA	108	104	2
TRKB	97	101	<1.0

TRKC	105	98	<1.0
TSSK2	95	92	2
TTK	96	107	156
TXK	90	81	14
TYK1/LTK	107	96	14
TYK2	90	93	<1.0
TYRO3/SKY	96	93	5
ULK1	98	98	3
ULK2	101	98	2
ULK3	104	104	<1.0
VRK1	106	96	4761
WEE1	100	101	ND
WNK2	93	93	2910
WNK3	97	93	ND
YES/YES1	81	76	2
ZAK/MLTK	100	92	ND
ZAP70	100	95	16
ZIPK/DAPK3	106	107	4

[a] GSK126 was tested in duplicate at a single dose of 10 μM.
[b] Staurosporine was used as a control compound and was tested with a 10-point 3-fold dilution series starting at 20 μM.
[c] ND, not determined.

1. Cheng,Y. & Prusoff,W.H. Relationship between the inhibition constant (K1) and the concentration of inhibitor which causes 50 per cent inhibition (I50) of an enzymatic reaction. *Biochem. Pharmacol.* **22**, 3099-3108 (1973).

Supplementary Table 5 | Growth IC$_{50}$ values, baseline H3K27me3 levels, mutation status, and tumor subtype for lymphoma cell lines.

Cell Line	Average Growth IC$_{50}$[a] (nM)	Baseline H3K27me3 level[b]	EZH2 Mutation Status[c]	Tumor Type[d]	Sub-Type[e]	t(14:18) Status[f]	p53 Status[g]	Cytostatic/ Cytotoxic[h]
WILL-2	27458	ND[i]	WT	B-NHL	DLBCL	N/A[j]	N/A	
Toledo	13786	34	WT	B-NHL	DLBCL	positive	mutant	
WILL-1	5527	ND	D185H[k] (Het)	B-NHL	DLBCL	N/A	N/A	
SU-DHL-4	4828	70	Y641S (Het); Y661N (Het)	B-NHL	DLBCL	positive	mutant	
RL	4727	55	Y641N; D185H (Het)	B-NHL	DLBCL	N/A	N/A	
U-2940	4558	ND	WT	B-NHL	DLBCL	N/A	N/A	
SU-DHL-8	3190	ND	WT	B-NHL	DLBCL	negative	mutant	
U-2932	2935	ND	WT	B-NHL	DLBCL	N/A	N/A	
SU-DHL-5	2299	39	WT	B-NHL	DLBCL	negative	WT	
Farage	1715	32	D185H (Het)	B-NHL	DLBCL	negative	mutant	
OCI-Ly-19	1019	23	WT	B-NHL	DLBCL	N/A	WT	
DB	861	63	Y641N (Het)	B-NHL	DLBCL	positive	mutant	cytostatic
SU-DHL-6	582	ND	Y641N (Het)	B-NHL	DLBCL	positive	mutant	cytostatic
HT	516	21	WT	B-NHL	DLBCL	negative	mutant	cytostatic
SU-DHL-10	448	134	Y641F (Het)	B-NHL	DLBCL	negative	mutant	cytotoxic
KARPAS-422	232	106	Y641N (Het)	B-NHL	DLBCL	positive	mutant	cytostatic
WSU-DLCL2	134	105	Y641F (Het)	B-NHL	DLBCL	N/A	mutant	cytotoxic
Pfeiffer	28	100	A677G (Het)	B-NHL	DLBCL	positive	WT	cytotoxic
Raji	7865	30	WT	B-NHL	Burkitt	N/A	N/A	
CA46	6585	28	D185H (Het)	B-NHL	Burkitt	N/A	N/A	
DG-75	3254	30	WT	B-NHL	Burkitt	N/A	N/A	
P3HR-1	3207	32	WT	B-NHL	Burkitt	N/A	N/A	
HS-Sultan	2275	26	WT	B-NHL	Burkitt	N/A	N/A	
Daudi	1265	55	WT	B-NHL	Burkitt	N/A	N/A	
Jiyoye	232	39	WT	B-NHL	Burkitt	N/A	N/A	cytostatic
BC-1	8292	20	WT	B-NHL	AIDS-BCBL	N/A	N/A	
BC-2	4762	24	WT	B-NHL	AIDS-BCBL	N/A	N/A	
BC-3	2217	36	D185H (Het)	B-NHL	PEL, AIDS-BCBL	N/A	N/A	
CRO-AP2	1643	ND	WT	B-NHL	PEL, AIDS-BCBL	N/A	N/A	
WSU-FSCCL	11966	ND	D185H (Het)	B-NHL	FL	N/A	N/A	
SC-1	3727	ND	D185H (Het)	B-NHL	FL	N/A	WT	
WSU-NHL	3537	ND	D185H (Het)	B-NHL	FL	positive	mutant	
NU-DUL-1	17060	ND	WT	B-NHL	N/A	N/A	mutant	
MC116	10168	39	WT	B-NHL	N/A	N/A	mutant	
RI-1	7656	ND	WT	B-NHL	MCL	N/A	mutant	
MINO	7340	ND	D185H (Het)	B-NHL	N/A	N/A	N/A	
U-698-M	5599	ND	WT	B-NHL	N/A	N/A	mutant	
MHH-PREB-1	5300	33	WT	B-NHL	N/A	N/A	mutant	
KARPAS-1106P	4536	ND	E744A (Het)	B-NHL	MLBCL	N/A	WT	
RC-K8	4528	40	D185H (Het)	B-NHL	N/A	N/A	WT	
CI-1	4282	ND	D185H (Het)	B-NHL	N/A	N/A	N/A	
SU-DHL-16	3282	ND	D185H (Het)	B-NHL	N/A	N/A	mutant	
HD-MY-Z	10717	30	WT	Hodgkin's	N/A	N/A	N/A	
L-428	4704	185	Y641S (Het)	Hodgkin's	N/A	N/A	N/A	
Hs 445	3528	32	WT	Hodgkin's	N/A	N/A	N/A	
RPMI-6666	1429	33	WT	Hodgkin's	N/A	N/A	N/A	

[a] Growth IC$_{50}$ values represent the average of at least 2 independent replicate experiments.

[b] Baseline H3K27me3 levels are represented relative to the level observed in the Pfeiffer cell line.

[c] Amino acid residue numbering based on NP_001190176.

[d] B-NHL, B-cell non-hodgkin lymphoma. Hodgkin's, Hodgkin's lymphoma.

[e] DLBCL, diffuse large B-cell lymphoma. Burkitt, Burkitt lymphoma. PEL, primary effusion lymphoma. AIDS-BCBL, acquired immunodeficiency syndrome body cavity-based lymphoma. MLBCL, mediastinal large B cell lymphoma. MCL, mantle cell lymphoma. FL, follicular lymphoma. N/A, not available.

[f] Deng et al., Cancer Cell 12: 171-185 (2007).

[g] Dornan et al., Blood 114: 2721-29 (2009).

[h] Dose-response curves from cell lines with growth IC$_{50}$ values < 1 μM were evaluated for evidence of cytostasis or cytotoxicity (values below T$_0$).

[i] Not determined.

[j] Not available.

[k] D185H is a known SNP (rs2302427).

Supplementary Table 8 | Common up-regulated genes in at least 4 out of 5 sensitive mutant cell lines[a]

Probeset ID	Symbol	Description	Entrez Gene	Unigene	Pfeiffer Fold Change	WSU-DLCL2 Fold Change	KARPAS-422 Fold Change	SU-DHL-10 Fold Change	HT Fold Change	SU-DHL-6 Fold Change	DB Fold change	OCI-LY-19 Fold Change	SU-DHL-4 Fold Change	Toledo Fold Change	Pfeiffer H3K27me3 Marked	KARPAS-422 H3K27me3 Marked	WSU-DLCL2 H3K27me3 Marked
201310_s_at	C5orf13	chromosome 5 open reading frame 13	9315	Hs.483067	2.68	2.04	4.65	2.39	1.55	1.45	2.24	1.06	1.01	1.09	No	No	No
201403_s_at	MGST3	microsomal glutathione S-transferase 3	4259	Hs.191734	2.16	3.30	2.49	2.68	1.64	1.93	1.41	1.28	1.34	1.05	Yes	Yes	Yes
201760_s_at	WSB2	WD repeat and SOCS box-containing 2	55884	Hs.719911	1.54	4.89	5.83	2.43	1.38	2.58	0.84	0.95	2.24	1.07	Yes	Yes	Yes
203504_s_at	ABCA1	ATP-binding cassette, sub-family A (ABC1), member 1	19	Hs.429294	3.66	1.56	11.38	2.73	1.81	2.59	2.56	0.86	1.03	0.97	Yes	Yes	Yes
203505_at	ABCA1	ATP-binding cassette, sub-family A (ABC1), member 1	19	Hs.429294	3.26	1.48	11.53	2.50	3.79	2.37	2.77	1.06	1.02	0.88	Yes	Yes	Yes
206857_s_at	FKBP1B	FK506 binding protein 1B, 12.6 kDa	2281	Hs.709461	2.39	2.90	11.45	4.52	2.79	2.64	1.69	3.37	2.33	1.34	Yes	Yes	Yes
207071_s_at	ACO1	aconitase 1, soluble	48	Hs.567229	2.02	3.68	0.82	2.67	2.08	2.01	1.13	1.44	1.70	1.37	Yes	Yes	Yes
208999_at	SEPT8	septin 8	23176	Hs.522057	0.87	2.43	4.42	21.93	1.71	4.81	1.44	1.75	2.45	1.10	No	No	No
209459_s_at	ABAT	4-aminobutyrate aminotransferase	18	Hs.336768	6.66	4.02	18.93	7.04	2.74	5.39	2.84	2.11	1.48	1.11	Yes	Yes	Yes
209504_s_at	PLEKHB1	pleckstrin homology domain containing, family B (evectins) member 1	58473	Hs.445489	2.63	6.62	4.45	2.88	1.79	2.92	1.95	1.68	1.53	1.00	Yes	Yes	Yes
209605_at	TST	thiosulfate sulfurtransferase (rhodanese)	7263	Hs.474783	2.52	4.52	3.20	2.84	1.90	3.45	1.05	1.10	1.83	1.10	Yes	Yes	Yes
209995_s_at	TCL1A	T-cell leukemia/lymphoma 1A	8115	Hs.2484	2.47	37.87	9.18	3.79	1.17	1.26	1.10	1.04	1.16	1.04	Yes	Yes	Yes
210778_s_at	MXD4	MAX dimerization protein 4	10608	Hs.655020	3.50	3.48	2.09	2.68	2.29	3.44	1.11	1.49	0.91	0.85	Yes	Yes	Yes
211474_s_at	SERPINB6	serpin peptidase inhibitor, clade B (ovalbumin), member 6	5269	---	2.02	2.02	1.11	5.86	2.87	2.95	1.12	1.61	2.13	1.46	Yes	Yes	Yes
212778_at	PACS2	phosphofurin acidic cluster sorting protein 2	23241	Hs.525626	1.63	2.58	3.01	2.33	1.59	3.15	1.26	1.73	1.28	1.09	Yes	Yes	Yes
213309_at	PLCL2	phospholipase C-like 2	23228	Hs.202010	3.21	2.17	1.95	3.01	1.82	2.03	1.05	1.16	2.07	0.92	Yes	Yes	Yes
213436_at	CNR1	cannabinoid receptor 1 (brain)	1268	Hs.709067	13.88	3.69	2.02	4.00	1.76	2.03	1.10	1.11	1.10	1.19	Yes	Yes	Yes
213901_x_at	RBM9	RNA binding motif protein 9	23543	Hs.282998	9.09	2.35	3.94	3.31	1.03	2.85	1.14	4.31	1.21	1.12	Yes	Yes	Yes
218175_at	CCDC92	coiled-coil domain containing 92	80212	Hs.114111	2.67	2.72	4.91	4.05	2.73	2.38	1.80	1.45	1.42	1.07	Yes	Yes	Yes
218346_s_at	SESN1	sestrin 1	27244	Hs.591336	2.29	6.75	1.62	4.84	2.41	2.73	1.58	1.50	1.95	0.99	Yes	Yes	Yes
218773_s_at	MSRB2	methionine sulfoxide reductase B2	22921	Hs.461420	2.53	4.68	4.86	4.69	1.72	6.19	1.69	1.43	1.74	1.10	No	Yes	Yes
219841_at	AICDA	activation-induced cytidine deaminase	57379	Hs.149342	2.43	3.16	18.71	1.53	1.26	2.34	3.56	1.87	1.17	3.35	Yes	No	Yes
221676_s_at	CORO1C	coronin, actin binding protein, 1C	23603	Hs.330384	2.13	2.56	2.87	2.88	1.77	1.62	1.49	1.84	1.06	1.02	Yes	Yes	Yes
221773_at	ELK3	ELK3, ETS-domain protein (SRF accessory protein 2)	2004	Hs.46523	3.88	2.29	1.69	2.36	1.32	3.01	1.81	0.92	0.93	1.09	Yes	Yes	Yes
222409_at	CORO1C	coronin, actin binding protein, 1C	23603	Hs.330384	2.02	2.31	3.08	2.47	1.58	1.72	1.65	1.51	1.02	1.02	Yes	Yes	Yes
224499_s_at	AICDA	activation-induced cytidine deaminase	57379	Hs.149342	2.53	3.04	27.88	0.47	1.27	2.46	1.15	0.65	1.22	0.98	Yes	No	Yes
225123_at	SESN3	sestrin 3	143686	Hs.659934	4.61	4.26	5.71	3.41	3.76	4.87	6.09	1.78	0.98	1.06	Yes	No	Yes
226272_at	RCAN3	RCAN family member 3	11123	Hs.656799	2.87	3.01	3.00	2.45	1.96	1.44	2.10	1.49	1.21	1.04	Yes	Yes	Yes
227001_at	NIPAL2	NIPA-like domain containing 2	79815	Hs.309489	2.73	2.86	2.90	2.90	1.13	2.30	1.20	1.24	1.33	1.02	Yes	Yes	Yes
227478_at	SETBP1	SET binding protein 1	26040	Hs.435458	2.76	5.63	3.32	2.04	2.38	2.11	1.83	0.37	1.73	1.53	Yes	Yes	Yes
228377_at	KLHL14	kelch-like 14 (Drosophila)	57565	Hs.446164	1.62	2.46	5.75	4.71	1.78	2.93	0.96	1.37	1.30	1.09	No	Yes	Yes
235352_at	---	---	---	---	3.33	2.24	6.47	2.16	1.63	1.99	1.18	1.37	1.49	0.94			
242448_at	MAP4K3	mitogen-activated protein kinase kinase kinase kinase 3	8491	Hs.655750	2.93	3.29	5.67	2.04	2.53	2.47	1.66	1.12	1.89	0.78	Yes	Yes	Yes
244166_at	APLN	apelin	8862	Hs.303084	1.31	5.52	5.33	5.38	1.36	2.12	1.48	1.12	1.56	0.73	No	Yes	Yes
39318_at	TCL1A	T-cell leukemia/lymphoma 1A	8115	Hs.2484	3.11	31.65	10.47	4.41	1.10	1.34	1.10	1.03	1.20	1.03	Yes	Yes	Yes

[a] Pfeiffer, KARPAS-422, WSU-DLCL2, SU-DHL-10, and SU-DHL-6.

Supplementary Table 9 |Significantly enriched gene ontology terms

Up-regulated probe sets only

GO Term	-Log$_{10}$(p-value) Pfeiffer	-Log$_{10}$(p-value) WSU-DLCL2	-Log$_{10}$(p-value) KARPAS-422	-Log$_{10}$(p-value) SU-DHL-10	-Log$_{10}$(p-value) SU-DHL-6
GOTERM_BP_5 GO:0007242 intracellular signaling cascade	3.15	2.11	1.67	1.20	2.11
GOTERM_MF_4 GO:0003779 actin binding	1.34	2.31	1.13	2.56	4.03
GOTERM_BP_3 GO:0012501 programmed cell death	2.67		2.34	3.11	
GOTERM_BP_3 GO:0050794 regulation of cellular process	4.03	1.28	2.75	2.25	3.26
GOTERM_BP_4 GO:0006915 apoptosis	2.78		2.19	3.34	
GOTERM_BP_4 GO:0048523 negative regulation of cellular process	3.07	2.52	2.11	3.92	2.49
GOTERM_BP_3 GO:0048519 negative regulation of biological process	2.90	2.80	1.98	3.82	2.67

Up- and down-regulated probe sets

GO Term	-Log$_{10}$(p-value) Pfeiffer	-Log$_{10}$(p-value) WSU-DLCL2	-Log$_{10}$(p-value) KARPAS-422	-Log$_{10}$(p-value) SU-DHL-10	-Log$_{10}$(p-value) SU-DHL-6
GOTERM_BP_4 GO:0048523 negative regulation of cellular process	4.07	4.02	2.55	3.26	2.86
GOTERM_BP_3 GO:0048519 negative regulation of biological process	3.54	4.14	2.28	3.02	3.00
GOTERM_BP_3 GO:0050794 regulation of cellular process	3.72	2.88	3.34	1.16	3.12
GOTERM_BP_4 GO:0007050 cell cycle arrest		2.24		2.15	3.46
GOTERM_MF_5 GO:0003714 transcription corepressor activity	2.64	2.16			2.36
GOTERM_BP_5 GO:0042981 regulation of apoptosis	2.52	3.08	2.24	1.58	
GOTERM_BP_5 GO:0043067 regulation of programmed cell death	2.45	2.99	2.16	1.53	
GOTERM_BP_3 GO:0050793 regulation of developmental process	2.12	2.63	2.23	3.09	1.07
GOTERM_MF_3 GO:0008134 transcription factor binding	2.00	3.51	1.51	1.17	2.85
GOTERM_BP_5 GO:0007242 intracellular signaling cascade	2.14	2.80	1.95	1.18	2.59
GOTERM_BP_5 GO:0051172 neg reg of nitrogen cmpd metabolic process	2.10	2.13	2.32	1.00	1.25